THREE COMPONENT VELOCITY MEASUREMENTS IN THE TIP VORTEX OF A MICRO-AIR-VEHICLE

THESIS

Hong Joon Park, Major, ROKAF

AFIT/GAE/ENY/06-S08

DEPARTMENT OF THE AIR FORCE
AIR UNIVERSITY

AIR FORCE INSTITUTE OF TECHNOLOGY

Wright-Patterson Air Force Base, Ohio

The views expressed in this thesis are those of the author and do not reflect the official policy or position of the United States Air Force, Department of Defense, or the U.S. Government.

AFIT/GAE/ENY/06-S08

THREE COMPONENT VELOCITY MEASUREMENTS IN THE TIP VORTEX OF A MICRO-AIR-VEHICLE

THESIS

Presented to the Faculty

Department of Aeronautics and Astronautics

Graduate School of Engineering and Management

Air Force Institute of Technology

Air University

Air Education and Training Command

In Partial Fulfillment of the Requirements for the

Degree of Master of Science in Aeronautical Engineering

Hong Joon Park, BS

Major, ROKAF

September 2006

AFIT/GAE/ENY/06-S08

THREE COMPONENT VELOCITY MEASUREMENTS IN THE TIP VORTEX OF A MICRO-AIR-VEHICLE

Hong Joon Park, BS

Major, ROKAF

Approved:

_____	_____
Dr. Mark F. Reeder (Chairman)	Date
_____	_____
Raymond C. Maple, Lt Col, USAF (Member)	Date
_____	_____
Paul A. Blue, Maj, USAF (Member)	Date

Abstract

An investigation into the characteristics of the wing tip vortex on a flexible wing micro-air-vehicle (MAV) was conducted. The Air Force Research Lab, Munitions Directorate designed a man-portable MAV with a 24” wingspan and 6” root chord to be used for battle damage assessment and reconnaissance or local surveillance. For this MAV, two prototypes have been produced. One has a rigid wing prepared from carbon-fiber; the other has a flexible wing prepared from parachute-latex material attached to a carbon-fiber frame. The experiments were performed to investigate the wing displacement and wing tip vortex interaction, characterizing the differences and effects of wing displacement and the shifting and velocity of wing tip vortex between two prototypes placed in typical operating conditions. Initially, each aircraft model was mounted at the test section in the low speed wind tunnel and exposed to various angles of attack and wind conditions. An optical telescope was used to measure the wing tip displacement and a tri-axial hot-wire anemometer was used to capture the velocity profiles in the wind tunnel to characterize wing tip vortex system. The results indicate that the wing tip displacement of the flexible wing was approximately 8 times than that of the rigid wing in an unstalled condition. The data suggests that flexible wing has a denser core-distribution of velocity within the wing tip vortex and delays the angle at which separation occurs.

Acknowledgments

Using this page, I would like to express sincerely my appreciation to my faculty advisor, Dr. Mark Reeder for his guidance support throughout the course of this work effort. Although had a lot of hard time to guide and teach me, he always obviously pointed the clear way and encouraged me and he also gave me deep consideration for my complicated situation. I would also like to appreciate, Dr. Michael OL in AFRL, for his support during this work. Dwight Gehring and John Hixenbaugh jr. spent a lot of time to model, set and perform this experiment and they gave a lot of technical advice to me. Last, I want to thank my wife and sons for showing me love and support I needed to successfully finish this work effort.

Hong Joon, Park

Table of Contents

Page

Abstract v
Acknowledgments vi
Table of Contents viii
List of Figures ix
List of Tables xii
List of Symbols xiii
I. Introduction 1
Background 1
Problem Statement 2
Research Objectives 3
Methodology 3
Preview 4
II. Literature Review 5
Overview 5
Flexible Wing MAVs 5
Wing Deformation/Aeroelastic effects 8
Wing Vortex system 10
Summary 17
III. Methodology 18
Overview 18
Test Subjects 18
Micro-Air-Vehicle 18
Telescopic Survey Tool 20
Wing Tip Displacement study *20*
Equipment/Test Setup 20
Experimental Procedure 21
Data Analysis 22

Page

Wing Vortex System Study 22
Equipment/Test Setup 22
Experimental Procedure 26
Data Analysis 29
Summary 29
IV. Analysis and Results 30
Overview 30
Wing Tip displacement Results 30
Wing Tip vortex System Results 34
Summary 56
V. Conclusions and Recommendations 62
Overview 62
Conclusions and Significance of Research 62
Future Recommendations 64
Appendix : Additional Data Results 66
Additional Velocity Contour Plots 66
Vita 74

List of Figures

Page

Figure 1. Flexible and Rigid Wing MAVs (DeLuca, 2004).....7

Figure 2. C_L & L/D vs. α for MAV (DeLuca, 2004).....7

Figure 3. MAV Flexible Wing Folded-up (Rivera Parga, 2004).....8

Figure 4. Wing deformation during Flight (nasa.gov).....8

Figure 5. C_L vs. α for varying Wing Stiffness (Ifju P.G et al, 2002:11).....9

Figure 6. Effect of downwash (aerospaceweb.org).....10

Figure 7. Generation of the trailing vortices due to load distribution (J. Bertin, 2002, Ch 7 : 232).....11

Figure 8. Geometry of Trailing Vortex.....13

Figure 9. Typical Shape of the Vortex (math.adelaide.edu.au).....14

Figure 10. Axial Velocity Data as a Function of Different Parameters.....16

Figure 11. Telescopic Survey Tool.....20

Figure 12. Telescopic Survey Tool Set Up.....21

Figure 13. AFIT Low Speed Wind Tunnel Schematic (DeLuca, 2004:26).....23

Figure 14. Wind Tunnel Test Section with Hot-wire Probe and Sting Balance.....24

Figure 15. Dantec 55P91 & 55R91 Triple Wire Anemometer (dantecdynamics.com).....25

Figure 16. Hot Wire Traversing System (B. Gamble, 2006:46).....26

Figure 17. Hot-Wire Test Grids from After View of MAV in Wind Tunnel.....26

Figure 18. Wing Tip Displacement Chart for Rigid Wing & Flexible Wing.....32

Figure 19. Interaction of Factors created on the Wing.....33

Figure 20. Axial Velocity as a Function of Angle of Attack.....36

Page

Figure 22. The Cross Velocity of the Vortex Core for the Flexible Wing.....38

Figure 23. Cross Velocity Magnitude as a Function of Angle of Attack.....39

Figure 24. Axial velocity near the center of the vortex as a Function of Circulation Parameter.....40

Figure 25. Velocity Profile of Left Wing Tip for Flexible Wing at 0° AOA.....41

Figure 26. Velocity Profile of Center Wing Tail for Rigid & Flexible Wing at 2°AOA..42

Figure 27. Velocity Profile of Center Wing Tail for Rigid & Flexible Wing at 4°AOA..43

Figure 28. Velocity Profile of Center Wing Tail for Rigid & Flexible Wing at 6°AOA..44

Figure 29. Velocity Profile of Center Wing Tail for Rigid & Flexible Wing at 8°AOA..45

Figure 30. Velocity Profile of Center Wing Tail for Rigid & Flexible Wing at 10° AOA.....45

Figure 31. Velocity Profile of Left Wing for Rigid & Flexible Wing at 2° AOA.....46

Figure 32. Velocity Profile of Left Wing for Rigid & Flexible Wing at 4° AOA.....47

Figure 33. Velocity Profile of Left Wing for Rigid & Flexible Wing at 6° AOA.....48

Figure 34. Velocity Profile of Left Wing for Rigid & Flexible Wing at 8° AOA.....48

Figure 35. Velocity Profile of Left Wing for Rigid & Flexible Wing at 10° AOA.....49

Figure 36. Velocity Profile of Left Wing Tip for Rigid & Flexible Wing at 2° AOA.....50

Figure 37. Velocity Profile of Left Wing Tip for Rigid & Flexible Wing at 4° AOA.....51

Figure 38. Velocity Profile of Left Wing Tip for Rigid & Flexible Wing at 6° AOA.....52

Figure 39. Velocity Profile of Left Wing Tip for Rigid & Flexible Wing at 8° AOA.....52

Figure 40. Velocity Profile of Left Wing Tip for Rigid & Flexible Wing at 10° AOA....53

Page

Figure 41. Finer Velocity Profile of Left Wing Tip for Flexible Wing at 0° & 2° AOA..55

Figure 42. Finer Velocity Profile of Left Wing Tip for Flexible Wing at 4° & 6° AOA..55

Figure 43. Finer Velocity Profile of Left Wing Tip for Flexible Wing at 8° & 10° AOA56

Figure 44. Variation Velocity Profile of Wing Tip for the Rigid Wing & Flexible Wing at 4° AOA.....58

Figure 45. Variation Velocity Profile of Wing Tip for the Rigid Wing & Flexible Wing at 8° AOA.....59

Figure 46. Variation Velocity Profile of Wing Tip for the Rigid Wing & Flexible Wing at 10° AOA.....60

Figure 47. Velocity Profile of Right Wing for Rigid & Flexible Wing at 2° AOA.....66

Figure 48. Velocity Profile of Right Wing for Rigid & Flexible Wing at 4° AOA.....67

Figure 49. Velocity Profile of Right Wing for Rigid & Flexible Wing at 6° AOA.....67

Figure 50. Velocity Profile of Right Wing for Rigid & Flexible Wing at 8° AOA.....68

Figure 51. Velocity Profile of Right Wing for Rigid & Flexible Wing at 10° AOA.....68

Figure 52. Variation Velocity Profile of Wing Tip for the Flexible Wing at 0°&2° AOA.....69

Figure 53. Variation Velocity Profile of Wing Tip for the Flexible Wing at 4°&6° AOA.....69

Figure 54. Variation Velocity Profile of Wing Tip for the Flexible Wing at 8°&10° AOA.....70

List of Tables

Page

Table 1. Core Velocity of previous Researches.....16

Table 2. Wing & Tail Geometric Properties.....19

Table 3. Performed Tests in Wind Tunnel.....29

Table 4. Wing Tip Displacement for Rigid Wing.....31

Table 5. Wing Tip Displacement for Flexible Wing.....31

Table 6. The Axial Velocity of the Vortex Core (U_∞ = 12.2783 *m/s*).....34

Table 7. Max Tangential Velocity magnitude of the Vortex.....38

List of Symbols

α	Angle of Attack
β	Sideslip Angle
mph	Mile per Hour
C_D	Coefficient of Drag
C_L	Coefficient of Lift
ρ	Air Density
U	Mean Velocity
U'	Standard Deviation of *u*-component of the Velocity
V	Vertical Velocity
W	Spanwise Velocity
L	Characteristic Length
Re	Reynolds Number
μ	Viscosity
ν	Kinematic Viscosity
u	Axial Velocity Component (Body Axis)
v	Vertical Velocity Component (Body Axis)
w	Spanwise Velocity Component (Body Axis)
x	Axial Coordinate (Body Axis)
y	Spanwise Coordinate (Body Axis)
z	Vertical Coordinate (Body Axis)
L/D	Lift and Drag Ratio
M_{ac}	Aircraft Mass
g	Gravitational Acceleration
S	Half-Spacing of the Trailing Vortices
V_{ac}	Aircraft Speed
Γ	Circulation
U_θ	Rotational Velocity
U_χ	Axial Velocity
r	Vortex core Radius
U_∞	Measured Freestream Velocity
U'_∞	Average Freestream Velocity
$U_{\chi,\max}$	Maximum Axial Velocity
ω	Angular Velocity
b	Wing Span

THREE COMPONENT VELOCITY MEASUREMENTS IN THE TIP VORTEX OF A MICRO-AIR-VEHICLE

I. Introduction

Background

In modern warfare, the collection and application of information are critically important. To coincide with this need, many nations have developed their own information assets. From this point of view, Unmanned Aerial Vehicles (UAVs) are well-suited. In these days, UAVs perform many tasks including surveillance, search & rescue, damage assessment reconnaissance and tactical attack missions. Predator, Global Hawk and Dark Star can be representative examples for these purposes. The need for inexpensive, the real-time surveillance at relatively short distances also arose. In order to meet this necessity, DARPA (Defense Advanced Research Projects Agency) defined a new category of UAVs, called Micro-Air-Vehicles (MAVs) (McMichael and Francis, 1997). These MAVs, which are much smaller and cheaper than current UAVs, could be used to perform various missions. They were designed to be a man-portable and can be used in special situations such as the image acquisition of short-distance enemy. And the resulting capability should be especially beneficial in the emerging urban war fighting environment, characterized by its complex topologies, confined spaces and areas (often internal to buildings), and high civilian concentrations (FAS, 2006). The Air Force Research Lab, Munitions Directorate, Flight Vehicles Integration Branch (AFRL/MNAV) developed a man-portable, carbon-fiber matrix UAV with a flexible wing of 24” span , 6” root chord , and 18.2” length. One important design goal is to

minimize the storage volume of the vehicle in order to improve its portability (Jose Rivera Parga and Mark F. Reeder et al, ref. 22, 2005). It has a flexible wing and can be folded to minimize its size and maximize portability in carrier's backpack.

Captain Anthony Deluca (USAF) studied the aerodynamic performance of the MAV and a rigid wing counterpart in order to report results in ref. 10. Two prototypes were experimented in wind tunnel to compare the characteristics. Wing flexure effects and control surface effectiveness were the focus of this study effort. Lieutenant Jose Rivera Parga (Mexico Navy) and Troy Leveron (US Navy) also performed wind tunnel tests on the MAVs at AFIT. They focused on the aerodynamic properties and flight qualities of the MAVs using a different tail. The results were reported in ref. 22 and ref. 21. Captain Brian J. Gamble (USAF) investigated the propeller-airframe interference effects and results were reported in ref. 17. Gamble also performed sets of three-component velocity measurement for a case where $\alpha = 0^{\circ}$.

Problem Statement

In the previous study, the measurements of the MAVs indicated that increased wing flexure delayed stall and increased the maximum value of L/D by approximately 20 to 30 percent for airspeeds ranging from 20 to 50 miles per hour (DeLuca, 2004). However some details are still unclear regarding what different changes occur in the flow field for the two wings in various conditions. Also the amount of wing displacement for this particular model was not measured in earlier work. The wing tip vortex is considered one of the important aerodynamic characteristics, and an investigation into its nature for the two different wings is the subject of this investigation.

Research Objectives

The objectives of this experimental study were to evaluate the wing tip displacement and the tip vortex characteristics of both the rigid and flexible wings exposed to various flight conditions. Experiments were performed in the wind tunnel to measure the wing tip displacement and characterize the wing's reactions including the wing tip vortex along with the changes of the aerodynamic conditions on each wing of the MAV.

Methodology

These objectives were accomplished by the following:

- Using a telescopic survey tool, measure the amount of wing displacement of two models in the AFIT wind tunnel along with the changes of angle-of-attack and velocity.

- Measure the changes of velocity profiles of two models using a three-component hot-wire with 140 *mm* x 180 *mm*, 160 *mm* x 180 *mm* and 80 *mm* x 120 *mm* grids and capture the velocity distribution to characterize the wing tip vortex system of the two models

This experimental study is focused to determine the wing displacement in the different given flight conditions. The variables were the angle-of-attack (α) which ranged from 0 to 10 degrees, and airspeed, varied from10 to 40 miles per hour (*mph*). Hot-wire measurements provide much more detail about the characteristic of the wing tip vortex for both rigid and flexible wings and also show displacement of the core taken at 30mph. Notably, sideslip angle (β) was not applied as a variable.

Preview

This document provides information about wing displacement and wing tip vortices for both rigid and flexible wing MAV. In Chapter II, some of the important research in the area is described. General information, theoretical analysis and experimental results are included. In Chapter III, the overall setup, methodology used to perform the experiment and procedures needed to make velocity profiles, data analysis are described with some pictures and references. Chapter IV presents the results gathered from each test and includes an analysis of the results. The conclusion of this research, entire summary and the suggestion for follow-on work are included in Chapter V.

II. Literature Review

Overview

The purpose of this chapter is to provide the basic concepts, engineering approaches and performed technologies related to wing displacement and the wing tip vortex. Furthmore this chapter includes the basic background of the flexible MAVs, the information of the aeroelastic effect wing displacement and also includes a description of the wing tip vortex system.

Flexible Wing MAVs

Practical applications of MAVs are becoming more achievable with the ever-decreasing size and weight of the payload components that can include video cameras, chemical sensors, electronics, and communication devices. And the present flexible wing technologies are developed to produce smooth flight even in gusty wind conditions. This flight characteristic is accomplished via the adaptive nature of the wing as well as its natural oscillation (Peter G. Ifju et al, 2002). This is the reason why the flexible wings are chosen for mentioned missions. The Reynolds numbers (*Re*), given in Equation 1, for most MAVs are in the range of 10^4 to 10^5. Such low Reynolds numbers make the problem of airfoil design difficult because the boundary layer is much less capable of handling an adverse pressure gradient without separation. Thus, very low Reynolds number designs do not have severe pressure gradients and the maximum lift capability is restricted (Desktop Aeronautics, 2006).

$$\text{Reynolds number } (Re) = \frac{inertia\ \ force}{viscous\ \ force} = \frac{\rho UL}{\mu} = \frac{UL}{\nu} \qquad \textbf{(1)}$$

Where:

ρ = fluid density
U = mean fluid velocity
L = characteristic length
μ = viscosity
ν = kinematic fluid viscosity: $\nu = \mu / \rho$

According to Peter G. Ifju (ref. 18), the adaptive washout is produced through twist of the framework and membrane and the shape changes of the flexible wing are demonstrated as a function of the airspeed and the angle of attack. As the plane hits a head-on wind gust the relative airspeed suddenly increases. The resulting increased dynamic pressure causes a shape change in the wing that decreases the lifting efficiency, but because the airspeed in the gust is higher, the wing maintains nearly the same lift. Once the airspeed decreases, the wing recovers to the original configuration.

Deluca, Reeder, OL and Freeman (ref. 11) investigated the aerodynamic properties of the flexible wing and analyzed these properties with the rigid wings, also studied control surface effectiveness. As a recent study effort, Gamble (ref. 17) demonstrated required power to run the MAVs with respect to loaded forces & moments and propeller interaction with the flexible wing. B. Gamble (USAF) included measurement of all three velocity components around the aircraft for one condition, $\alpha = 0°$.

Two models in Figure 1 were investigated at the AFIT wind tunnel and the design of the models had been changed several times to perform the ideal missions.

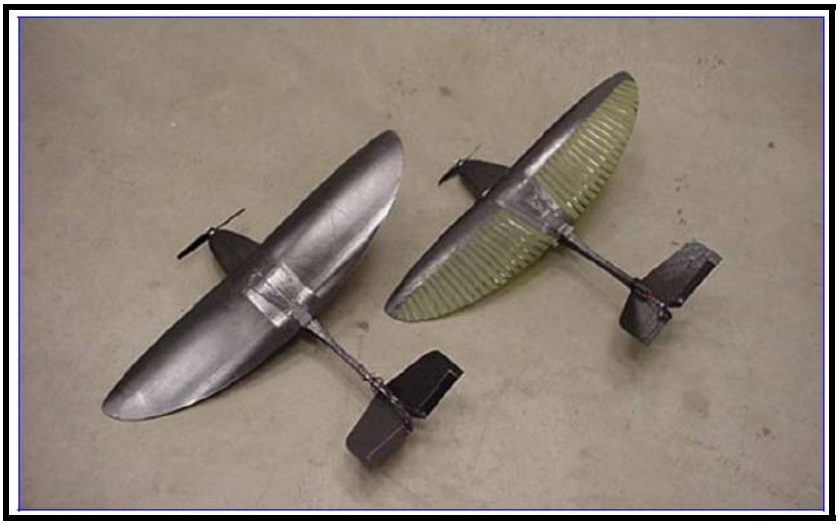

Figure 1. Flexible and Rigid Wing MAVs (DeLuca, 2004)

Captain DeLuca tested the two models in the Figure 1 to determine aerodynamic properties such as lift, drag, L/D, and moments, and reported the results for the two models. In the results, shown in Figure 2, flexible wing has higher L/D values in most range of angle-of-attack and velocities. This information indicates that flexible wing is more suitable for the MAV since it produced better aerodynamic characteristics.

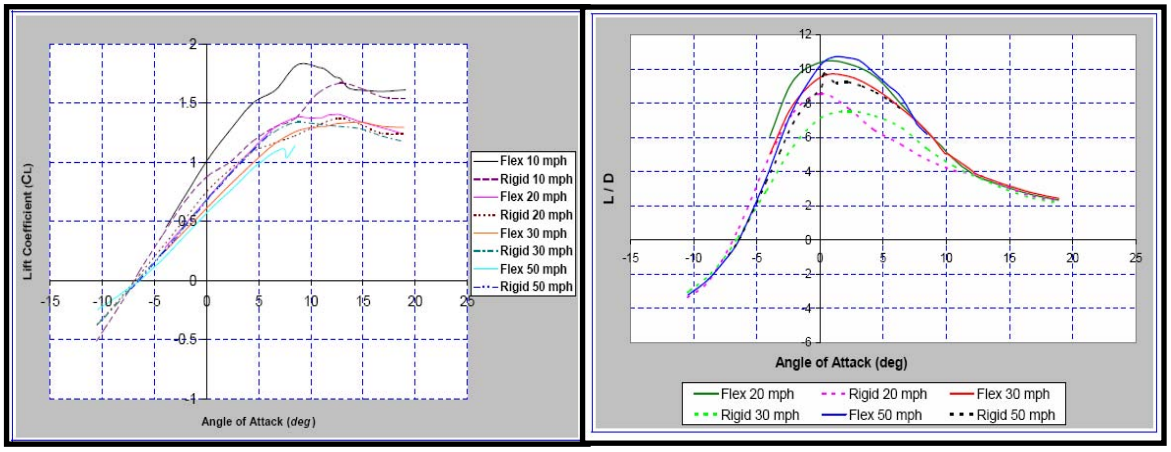

Figure 2. C_L & L/D vs. α for MAV (DeLuca, 2004)

In the view of operation, the MAV built in flexible wing can be folded to maximize portability and to minimize size as seen in Figure 3.

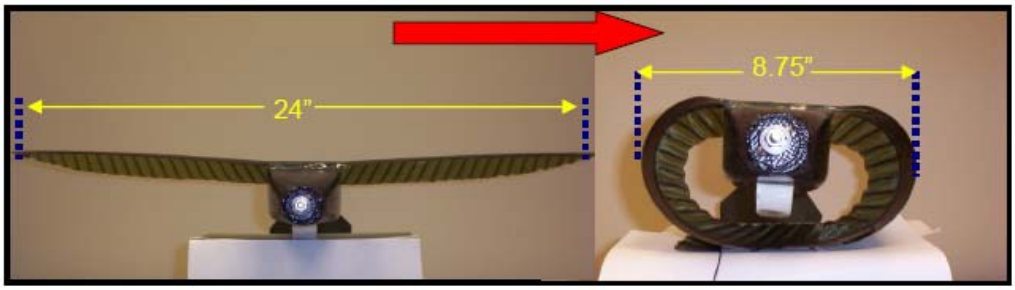

Figure 3. MAV Flexible Wing Folded-up (Rivera Parga, 2004)

Wing deformation/Aeroelastic effects

All aircraft have elastic deformation at wings, control surfaces and fuselage during flight. Modern aircraft constructed of light materials have more elastic deformation during flight. In Figure 4, the uninhabited aerial vehicle which is researched in NASA, Helios, is composed of ultra light composite materials. This air vehicle clearly shows the example of wing deformation due to pressure distribution.

Figure 4. Wing deformation during Flight (nasa.gov)

And this character directly affects the aerodynamic nature of the MAVs. This deformation occurs based on aeroelastic effect. Aeroelastic effect is defined as the interaction between an elastic structure and a surrounding flow. Some elastic wings were tested by Ifju et al to show the usefulness of aeroelastic effects. In Figure 5, this data came from different MAV but the model in Figure 5 has very similar structure and materials to AFIT flexible model. The result indicated that the elastic wing allows the vehicle to achieve higher angle-of-attack without stalling. This fact coincides with significant static deformation of the wing under load, particularly at high angle-of-attack (W. Shyy, 2005).

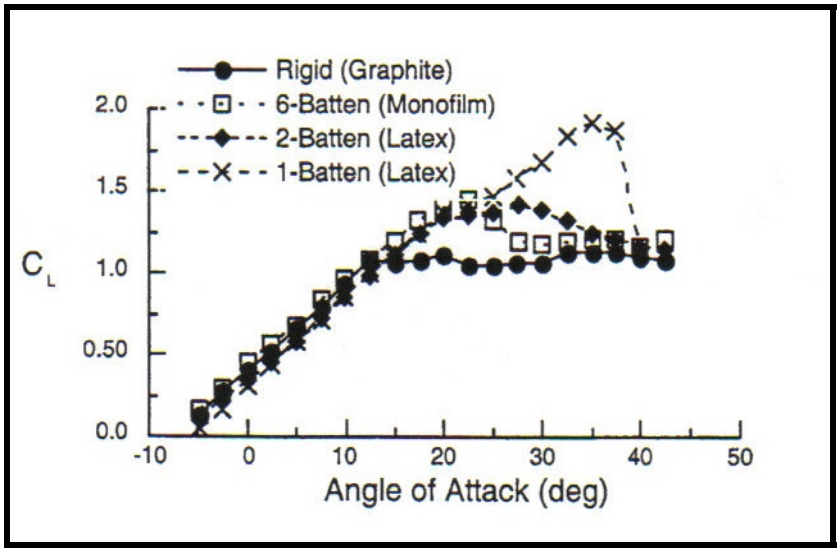

Figure 5. C_L vs. α for varying Wing Stiffness (Ifju P.G et al, 2002:11)

Wing Vortex system

A lifting wing produces the downwash in Figure 6 comes off the wing as a sheet and is related to the load distribution on the wing. The distribution of load changes from the root of the wing to the tip during maneuvering as seen in Figure 7. Thus, the amount of air in the downwash must also change along the wing. Since the wing near the root is diverting so much air the net effect is that the downwash sheet will begin to curl outward around itself, just as the air bends around the top of the wing because of the change in the velocity of the air. This is the wing vortex. The tightness of the curling of the wing vortex is proportional to the rate of change in lift along the wing. At the wing tip the lift must rapidly become zero causing the tightest curl. This is the wing tip vortex and is well represented in Figure 7 and described in many textbooks.

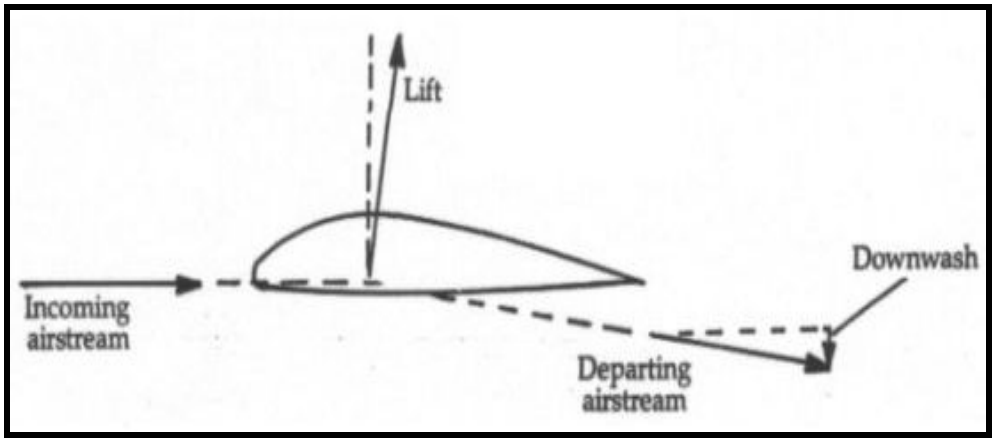

Figure 6. Effect of downwash (aerospaceweb.org)

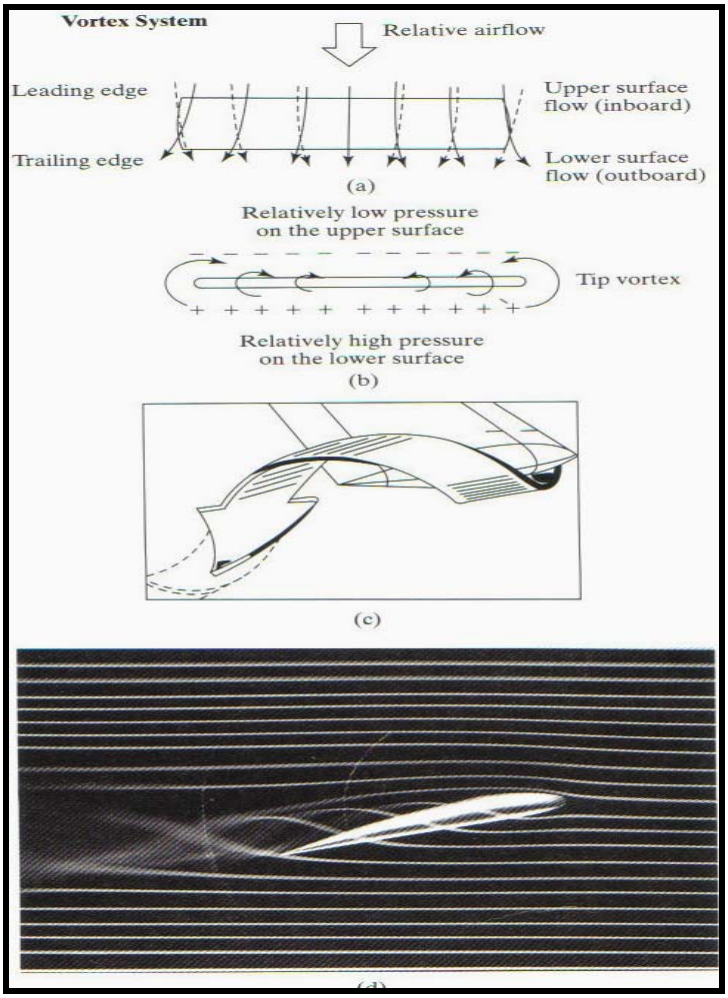

Figure 7. Generation of the trailing vortices due to load distribution (J. Bertin, 2002, Ch 7 : 232)

In 1858, Helmholtz summarized some of the properties of vortex filaments, or vortices.

These three theorems govern the behavior of inviscid three-dimensional vortices:

1. Vortex strength is constant.

2. Vortices are forever (end on boundaries or form a closed path).

3. Vortices move with the flow.

In steady level flight, the downward rate of change of vertical momentum of the air is matched by the lift on the aircraft (S. Bradley, 2005). The Kutta-Joukowski Lift Theorem gives lift per unit length as

$$\frac{M_{ac}\, g}{2S} = \rho V_{ac}(2\Gamma) \qquad \textbf{(2)}$$

where M_{ac} is the aircraft mass, g is the gravitational acceleration, S is the half-spacing of the trailing vortices, ρ is air density, V_{ac} is aircraft speed, Γ is the circulation associated with one of the trailing vortices (Anderson, J. D.,2001). The vortex spacing, 2S, is about $\pi/4$ of the wing span (Dougherty et al, 2004) for an elliptically loaded wing.

The tip vortex system can be considered in terms of rotational velocity (U_θ) and axial velocity (U_χ). In a generic vortex U_θ is related to circulation and distance (*r*) to the core by Equation (3a). In Figure 8, rotational velocity at a distance *r* is

$$U_\theta = \frac{\Gamma}{2\pi r} \qquad \textbf{(3a)}$$

This equation is the simplest approximation for incompressible uniform flow and no ground surface. By (3a), rotational velocity is proportional to circulation and inversely proportional to radius. In other words, rotational velocity is larger near the core of vortex than at the outside of core. This equation is not complete enough to describe

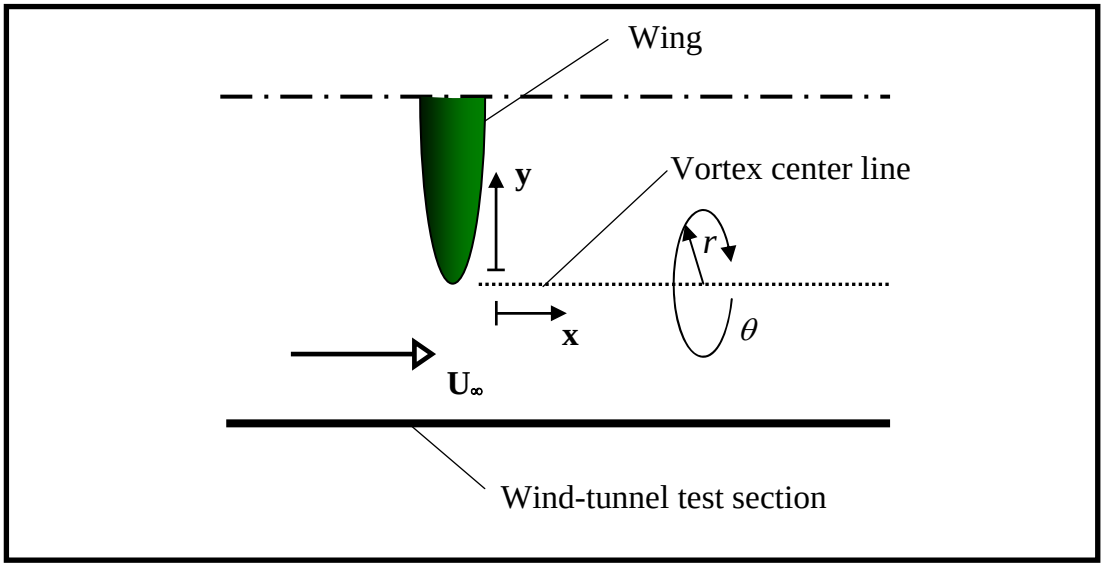

Figure 8. Geometry of Trailing Vortex

total rotational velocity of vortex but very useful to understand the vortex behavior. Other more realistic vortex models include the Oseen vortex (Rossow, V. J., 1999) with

$$U_\theta = \frac{\Gamma}{2\pi r}\left(1 - e^{-\frac{r^2}{r_0^2}}\right) \qquad \textbf{(3b)}$$

or

$$U_\theta = \frac{\Gamma}{2\pi}\frac{r}{r^2 + r_0^2} \qquad \textbf{(3c)}$$

(Burnham and Hallock, 1982), which give a vortex core of width about $r = \pm r_0$ where the velocities are reduced. Equations (3b) and (3c) also describe rotational velocity comes to be gradually slow as increases. An excellent review of trailing vortices is given by Spalart (ref. 25). One point regarding axial flow U_χ raised by Spalart is of keen interest, as follows

" The axial flow has a rich behavior, may sustain small-scale turbulence, and could also be essential in detecting trailing vortices from behind. It has surprised many of us that the velocity relative to the atmosphere may be directed towards the airplane but also away from it ("jet-like"). Jet-like flow gives an apparent thrust in a control-volume equation, which is offset by low pressure in the same region. I consider inviscid incompressible flow. The first explanation uses the shape of the vortex lines. After leaving the trailing edge, the weaker regions of the vortex sheet are wrapped around the vortices that are forming, primarily at the tip. This gives the vortex lines a helical shape, a right-hand helix for the right wing. This is what induces jet-like axial flow, peaking on the vortex axis and zero outside the outer turn of the vortex sheet. Such flow is related to rotational flow because in a steady flow the vortex lines and the streamlines coincide."(R. Spalart, 1998).

Figure 9. Typical Shape of the Vortex (math.adelaide.edu.au)

According to R. Spalart (ref. 25), the coincidence of vortex lines and streamlines is expressed by $\omega_x u_\theta = \omega_\theta u_x$, where ω is angular velocity. This equation can be written as

$$\frac{d\left(u_x^2 + u_\theta^2\right)}{dr} + \frac{2u_\theta^2}{r} = 0 \qquad \textbf{(4)}$$

If the circulation at radius *r* is denoted by $\tilde{\Gamma} = 2\pi r u_\theta$, equation (4) can be rewritten as

$$\frac{4\pi^2 r^2 d\left(u_x^2\right)}{dr} + \frac{d\left(\tilde{\Gamma}^2\right)}{dr} = 0 \qquad \textbf{(4a)}$$

The bottom line of the equation (4a) is that because $\left|\tilde{\Gamma}\right|$ increases with *r*, $\left|u_x\right|$ increases as the vortex axis is approached. Additionally, considering in terms of pressure, r momentum equation is

$$\frac{dp}{dr} = \frac{u_\theta^2}{r} \qquad \textbf{(5)}$$

And Bernoulli equation is

$$\frac{d\left(p + \left[u_x^2 + u_\theta^2\right]/2\right)}{dr} = 0 \qquad \textbf{(6)}$$

Combining equations (5) and (6), equation (4) is derived and overall taking above equations into account, the core has low pressure and high velocity. Green (1995) reported u_x/U_∞ = 1.62. S. Chow et al (1997) measured u_x/U_∞ = 1.78 for a rectangular wing at 10° angle of attack. Their results and those of two additional researchers are given in Table 1.

reference	Core U_{χ}/U_{∞}	Comment
Chow et al	1.78	*x/c* = -0.005 (just upstream of the trailing edge)
De Bruin	1.06	*x/b* = 0.7
Green	1.62	$\Gamma/(U_{\infty}b) \approx 0.14$
Anderson &Lawton	0.8 to 1.4	Dependence on circulation parameter

Table 1. Peak Vortex Core axial velocity of previous Researches

Where Γ is measured circulation and *b* is a wing span. Green used circulation parameter in his work instead of the position of measurement. Anderson and Lawton tested a NACA 0015 wing model to investigate the trailing vortex system in wind tunnel and reported the result in his study (ref. 2) as seen in Figure 10.

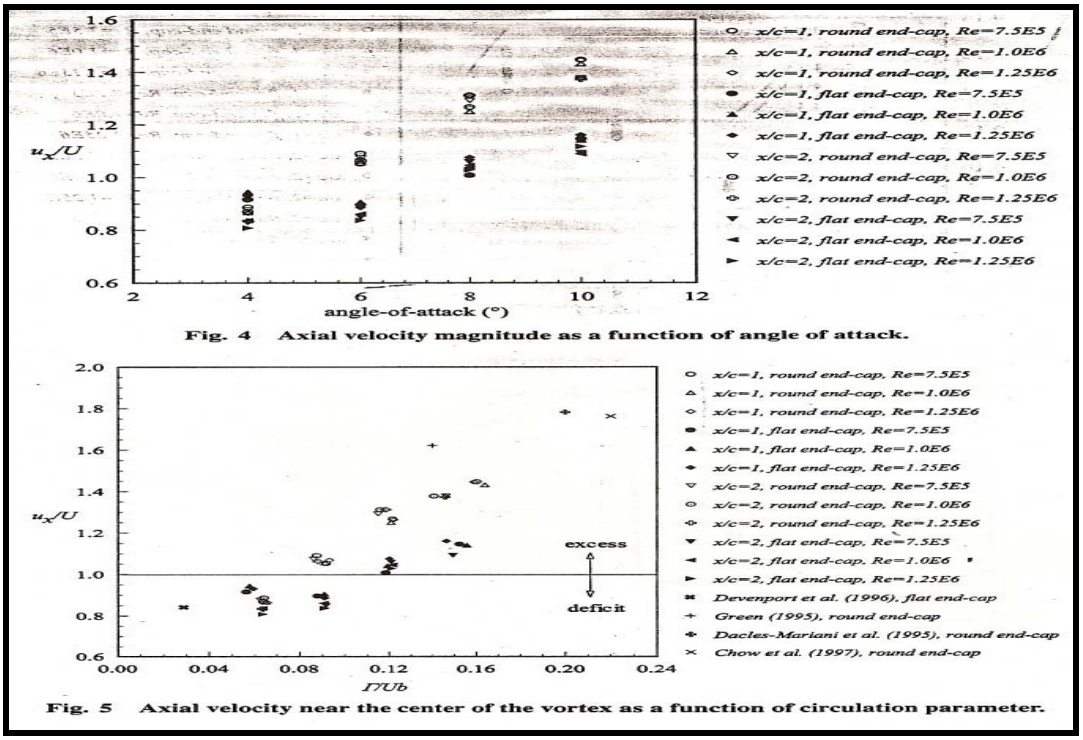

Figure 10. Axial Velocity Data as a Function of Different Parameters (Anderson and Lawton, 2003)

Where Γ is the measured circulation strength and *b* is twice the model semispan. In this result, the value of U_x is directly proportional to not only angle of attack but also circulation parameter and increased axial velocity can exceed the freestream velocity by as much as 70%.

Summary

The development of current MAVs and the concepts of flexible wing were described in Chapter II. It is also presented information and basic concepts from previous research in the field of aero elasticity and vortex system. Specially, the conception of each velocity component in vortex system will be importantly utilized to understand the comparison between rigid wing and flexible wing.

III. Methodology

Overview

This chapter fully describes the equipment, experimental procedures and data analysis used in the MAV wing tip displacement and wing vortex system experiments. Two separate tests were conducted in wind tunnel. The first set of experiments was designed to measure the wing tip displacement for two MAV models in wind tunnel as a function of freestream velocity and angle of attack. The second test was also conducted in the low speed wind tunnel where MAV velocity profiles were gathered using a three-component hot-wire anemometer.

Test Subjects

Micro-Air-Vehicle

The vehicles being tested in this experiment are the MAVs shown in Figure 1. The fuselage is composed of a carbon fiber matrix and has room to keep some electrical devices; motor, actuators, batteries, etc. The wing, whether rigid or flexible, is high mounted on the fuselage. The control surfaces attached to a V-tail are a combination of elevators and rudder (ruddervators). In all tests, the control surfaces (ruddervator) were set to zero degree deflection. The rigid and flexible wings both have the same geometric planform and each wing was attached to body by chemical glue. The rigid wing is completely constructed of carbon fiber but the flexible wing was constructed of a carbon fiber matrix leading edge. Carbon fiber ribs attached orthogonally to the leading edge

support a parachute-latex membrane forming the rest of the wing surface. Table 2 summarizes the geometric properties of the wing and tail surface.

Specification	Wing	Specification	Tail
Area	93.5 in^2	Area	14.8 in^2
Root Chord	6"	Chord	2.35"
Mass – flexible, rigid	0.705 lb_m, 0.794 lb_m		
Mean Aerodynamic Chord (c_{bar})	4.2"		
Span	24"	Span	6.3"
Carbon Fiber Leading Edge Thickness	0.025"	Thickness	0.03"
Parachute Planform Thickness	0.005"		
Aspect Ratio	6.16	Aspect Ratio	2.7

Table 2. Wing & Tail Geometric Properties

Telescopic Survey Tool

In order to measure the wing tip displacement, the fine traverse with a telescope and minute ruler which has the scale of the mode of the dial was utilized as seen in Figure 11 at the wind tunnel test section. This telescope consists of three parts; objective lens, telescope tube and eyepiece lens. Before using that optical instrument, the base of the telescope was mounted into a fixed position. During the tests, the telescope was vertically controlled by a dial scale connected to screw-type-gear and horizontally controlled by finer controller. The value measured from telescope tool was displayed on digital window box electrically connected to dial scale.

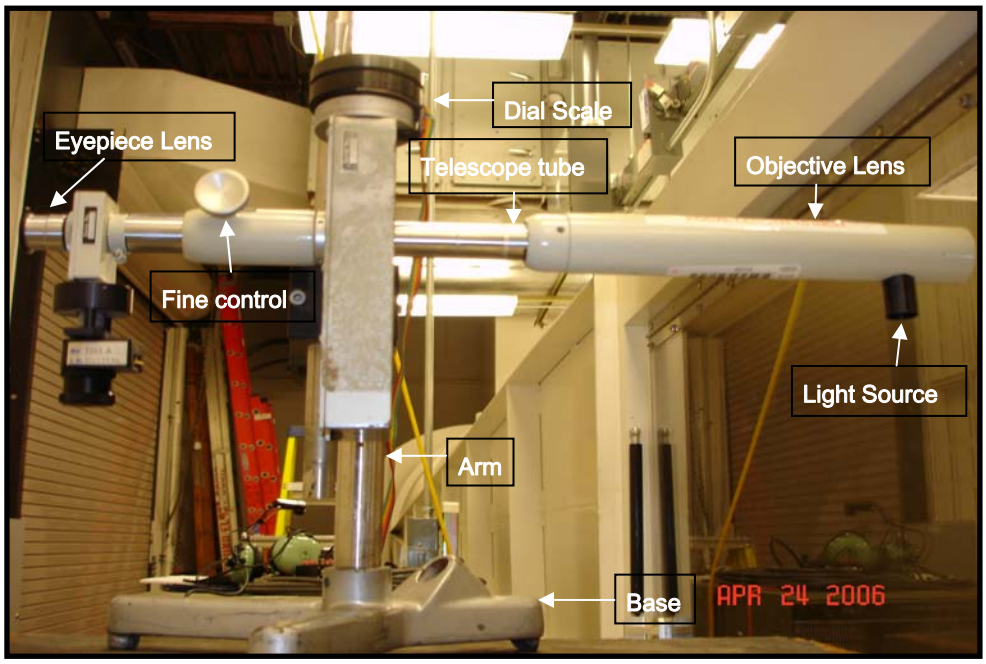

Figure 11. Telescopic Survey Tool

Wing Tip Displacement Study

Equipment/Test Setup

The purpose of this test was to measure the wing tip displacement along with the changes of freestream velocity & angle of attack. In order to accomplish this, each MAV model was placed in the wind tunnel test section, and then telescopic survey tool was placed right outside of the test section window as seen in Figure 12.

Figure 12. Telescopic Survey Tool Set Up

Several external lights were utilized to illuminate the model, and before performing the experiment, the outermost ends of the rounded wing tip of two models were marked with white color. Before every measurement performed, the scale of the telescopic survey tool was set to zero to analyze the absolute value of every wing tip displacement.

Experimental Procedure

After the setup was done, the testing began. The start point was from zero displacement in the wind tunnel with zero angle of attack and zero freestream velocity. Once the desired freestream velocity was reached, each wing tip displacement was measured from 0° to 10° angle of attack. This procedure was conducted from 0 mph to 40 mph freestream velocity for both rigid wing and flexible models. While measuring the wing tip displacement, there was a vibration at the wing tip. The middle value of

vibration range was selected as an effective value. This limitation could be improved upon by analyzing the data after visually recording the vibration in the future.

Data Analysis

For this set of tests, data achieved by telescopic survey tool were manually collected by reading the measured value displayed on the digital window. The collected data were stored in Microsoft® Excel program to be analyzed symmetrically and visualized. These results including plots and tables are presented in Chapter IV for both rigid wing and flexible wing model.

Wing vortex system Study

Equipment/Test Setup

The purpose of the second phase of testing was to investigate the wing efficiency of two models and compare the wing tip vortex system effects on the MAVs in the wind tunnel. For this test, hot-wire measurements were taken using a triple-wire anemometer to provide velocity profiles at multiple locations about the MAV.

The AFIT 3'x3' low speed wind tunnel, located in building 644 room L154, was constructed by Aerolab. It is an open circuit wind tunnel that draws in air from within the room. It has a design speed of 150 *mph* and has been tested at 148 *mph* (B. Gamble, 2006). A schematic of the wind tunnel is shown in Figure 13.

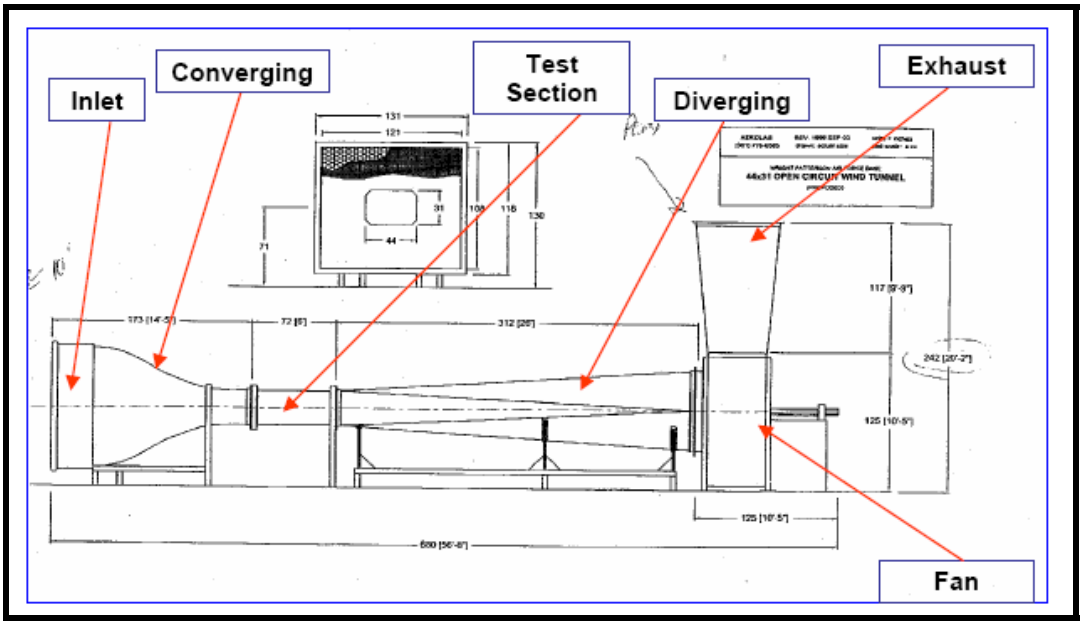

Figure 13. AFIT Low Speed Wind Tunnel Schematic (DeLuca, 2004:26)

The open-circuit wind tunnel intake plenum has dimensions of 122"w × 111"h ×70"d and is fitted with a 1/4" aluminum honey comb flow-straightener and 20"×20" steel mesh anti-turbulence screens. The converging section has a contraction ratio of 9.5:1. The test section measures 72” long by 44” wide by 31” high. The top and sides of the test section are constructed of Plexiglas and can be opened for test section access. The test section is 31"w × 44"w × 72"l. The MAV span-to-tunnel width ratio is b/w = 24"/44" = 0.55, where the generally accepted rule of thumb is $b/w \leq 0.8$ (B. Barlow et al, 1999, Ch 2:28).

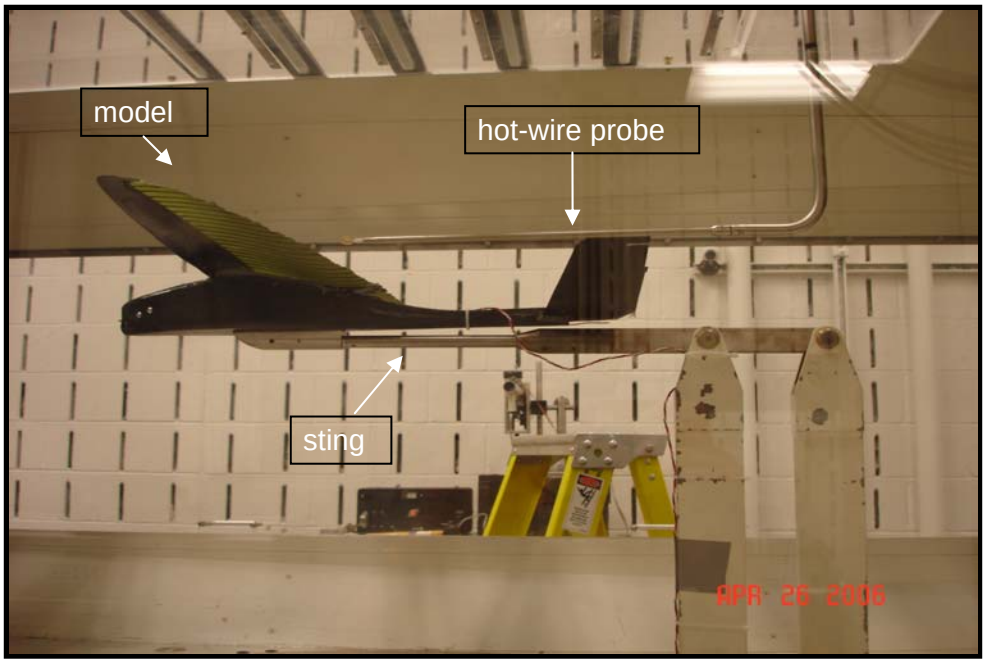

Figure 14. Wind Tunnel Test Section with Hot-wire Probe and Sting Balance

The model support sting enters the tunnel through a slot at the bottom of the test section. In Figure 14, it can traverse angles of attack from -20° to + 20°, and sideslip angles from -15° to +15°. It includes the sting with the balance mounted on the sting support and the hot-wire probe extending in from the top of the tunnel (B.Gamble, 2006)

In order to provide velocity profiles around the MAV, a Dantec Dynamics Streamline 55P91 tri-wire anemometer was used. It provided velocity measurements in all three axes (*u*,*v*,*w*) with respect to the tunnel. The three components are important when studying the three-dimensional flowfield. The tri-wire is shown in Figure 15. The probe has three mutually perpendicular sensors, consisting of gold-plated wires that form an orthogonal system with an acceptance cone of 70.4°. The wire ends are all perpendicular to the sensors with a diameter of 5 μm and length of 1.25 *mm* that lie within

a 3 *mm* sphere (dantecdynamics.com). Its nominal velocity limits are 0.05 *m/s* to 200 *m/s*.

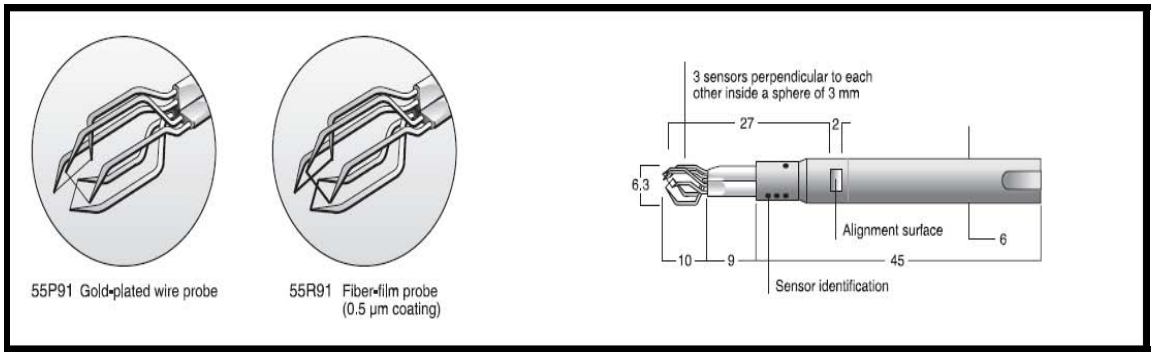

Figure 15. Dantec 55P91 & 55R91 Triple Wire Anemometer (dantecdynamics.com)

This was the second time this triple wire system had been used at AFIT and it had to be calibrated. Before start this study, Mr. Dwight Gehring and Capt Brian Gamble performed the calibration at previous experiment. This calibration process is described well in ref. 17.

The tri-wire was mounted to a probe that extends down from the top of the tunnel through the open slots and was attached to a Dantec fully automatic and programmable traversing system. This system allows the probe to capture the three components of velocity automatically with a pre-planed grid without disturbance to freestream. The traversing system is shown in Figure 16.

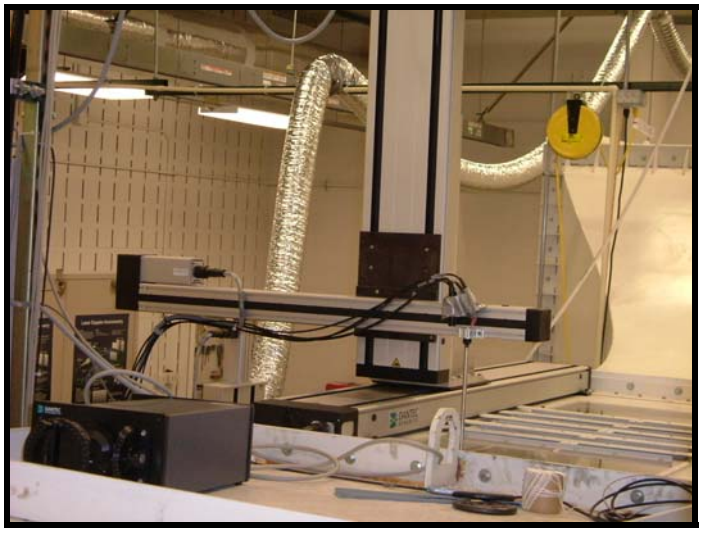

Figure 16. Hot Wire Traversing System (B. Gamble, 2006:46)

Experimental Procedure

Before starting the first set of tests, the hot-wire was mounted properly and set in the traversing system and rigid wing model was mounted first on the sting in the test section and propeller was removed to investigate the efficiency of only wings during all tests. Also, to capture the velocity profile independently, pre-planed grids were loaded on the control computer. The hot-wire was perpendicularly mounted in the wind tunnel so air flow in the wind tunnel was parallel to the *u*-component of the hot-wire.

After all setup was done, the measuring instrument was moved to the origin for traversing. It was set as far out on the left wing as the slot would allow and just over 3" below the trailing edge of the wing. Three grids were utilized in order to acquire each velocity component and additionally, one finer grid was utilized to measure the vortex displacement and density. Two large grids, one on each side of the wing, were developed to span 180 *mm* up and 140 *mm* across. One small grid, one on top of the v-tail, was

developed to span 120 *mm* and 80 *mm* across. The traversing system uses metric units and data was taken at 10 *mm* increments. Due to the physical constraints of the v-tail and the sting, data could not be collected from several small areas. This was a limitation of this experiment and this limitation can be removed using a smaller velocity acquisition system. The grids used in the wind tunnel and constraints are illustrated in Figure 17. Since all experiments are conducted in the wind tunnel, it also could be a limitation that the applied conditions in the wind tunnel are comparatively more ideal than in nature.

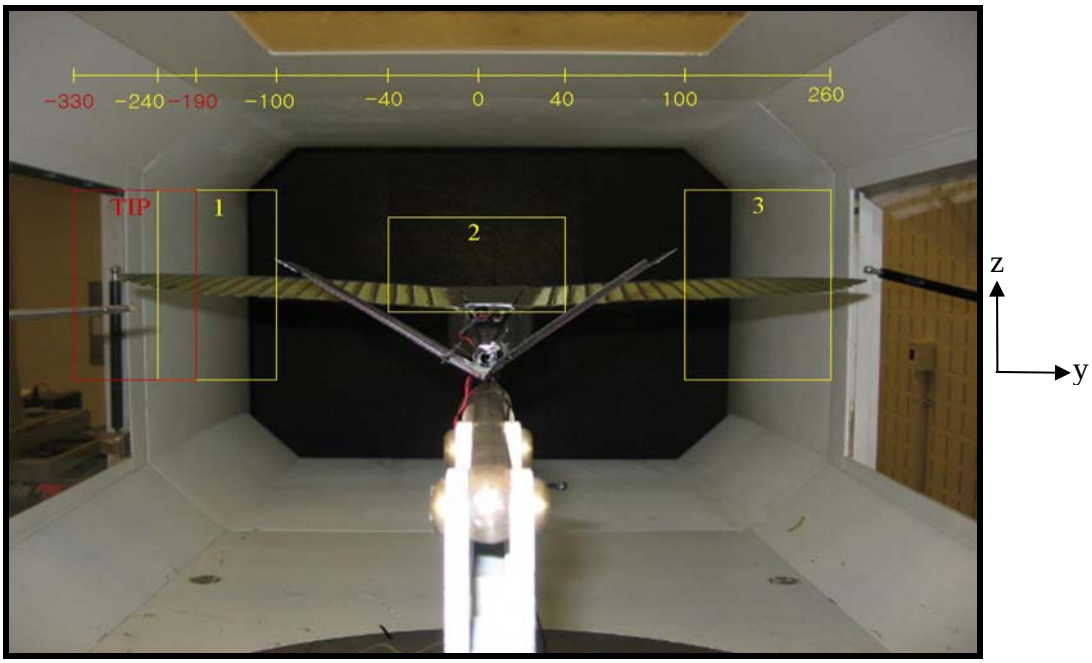

Figure 17. Hot-Wire Test Grids from After View of MAV in Wind Tunnel

Another limitation was that in its original configuration, the hot-wire probe could not reach to outer part of wing tip due to wind tunnel configuration. But the acquisition of velocity components near the wing tip was essential part of this study investigating the

wing tip vortex system. Therefore to solve this limitation, the probe was rotated 18.5° about z-axis. This rotation was in the operation limits of hot-wire probe (acceptance cone 70.4°) and the data achieved from rotated probe were numerically corrected in Chapter IV. The first test was started for rigid wing from 2° angle of attack, 30 *mph*. This corresponds to a Reynolds number based on mean chord of about 1.3×10^5 and Mach number of 0.038. All tests conducted in the wind tunnel for vortex system were performed with 30 *mph* airflow only. The acquisition of velocity components was automatically performed by traversing system according to the grid selected but each grid had to be selected manually. Once all of the tests for the rigid wing model were completed, the rigid wing was detached from planform, and then the flexible wing was attached to planform by chemical glue. It took one day for the glue to dry. After that, the same tests were conducted on the MAV with flexible wing. The finer grid was utilized for only flexible wing model to detect the finer velocity components to investigate the wing tip vortex characteristics in additional detail. This finer grid has the same size with large grid used in previous tests but has smaller increments (5 *mm*) than those of the previous grids. Table 3 shows the tests conducted for two models in wind tunnel.

Model / Velocity	Rigid Wing	Flexible Wing
30 mph	· 2° to 10° AOA (2° increments) · Wing Tip · Left Wing · Right Wing · Top of v-tail	· 0° to 10° AOA (2° increments) · Wing Tip · Left Wing · Right Wing · Top of v-tail · Wing Tip with finer grid

Table 3. Performed Tests in Wind Tunnel

Data Analysis

For the wind tunnel tests, the data collected through the hot-wire probe were saved using Dantec Streamware® operation software. The raw data included both the mean and standard deviation of *u*, *v*, and *w* velocity components in *m/s*. These measurements were achieved while hot-wire probe stopped for 5 seconds at each grid point at a rate of 1 kHz. To analyze the saved data, the raw data had to be manipulated in other software. So the raw data were manipulated in Microsoft® Excel. Each raw data set has its own origin. The individual coordinates were switched to match the wind tunnel coordinates seen in Figure 16. The wingtip velocity data was numerically transformed to account for the 18.5° rotation in the hot-wire probe. All of manipulated data were plotted in Tecplot®. These plots are presented in Chapter IV.

Summary

Chapter III presented the equipment, test subjects, experimental procedures, some limitations and data analysis used in both wing tip displacement study and wind tunnel study for vortex system. Figures and tables were provided to understand each experimental test setup and procedure performed the wind tunnel. All of tests completed in this study were described in Chapter III and the results from tests are presented in Chapter IV.

IV. Analysis and Results

Overview

This chapter details the results of the wing tip displacement test and vortex system in wind tunnel. Graphical representation illustrates the wing tip displacement of each model. Velocity profiles taken in the wind tunnel show the characteristics of varied angles of attack for each wing. These results are compared to the literature and analyzed.

Wing tip displacement Results

Wing displacement can be presented as a function of angle of attack and the material stiffness of the wing. It is predicted easily that the stiffness of the rigid wing is higher than the stiffness of the flexible wing. By definition the flexible wing has more deformation than rigid wing. Table 4 shows the results of the mean wing tip displacement for rigid wing and Table 5 shows the results of the wing tip displacement for flexible wing under the conditions tested. The vibration level was smaller in the flexible wing than in the rigid wing and such phenomenon was prominent in especially high angle of attack. This means that the pressure distribution is more stable on the flexible wing while the rigid wing is more influenced from turbulence effect according to separation generated earlier. This inclination is graphically presented in wing vortex system results part. Although the vibration taken place at the wing tip during testing is not presented carefully in this study but the vibration was observed less in flexible wings

than in rigid. In this study, the accuracy of the instrument used for the measurement is 0.001 mm.

MPH / AOA	10	20	30	40
0°	0.000 mm	0.256 mm	0.479 mm	0.649 mm
2°	0.030 mm	0.299 mm	0.712 mm	1.137 mm
4°	0.042 mm	0.424 mm	0.867 mm	1.512 mm
6°	0.058 mm	0.827 mm	1.308 mm	2.199 mm
8°	0.060 mm	1.946 mm	2.227 mm	3.462 mm
10°	0.128 mm	1.041 mm	1.890 mm	3.215 mm

Table 4. Wing Tip Displacement for Rigid Wing

MPH / AOA	10	20	30	40
0°	2.129 mm	4.639 mm	8.419 mm	12.752 mm
2°	2.260 mm	5.776 mm	10.657 mm	16.638 mm
4°	2.657 mm	6.533 mm	12.265 mm	20.100 mm
6°	2.726 mm	7.802 mm	14.650 mm	23.732 mm
8°	3.500 mm	8.664 mm	16.588 mm	27.525 mm
10°	3.564 mm	8.751 mm	18.056 mm	30.223 mm

Table 5. Wing Tip Displacement for Flexible Wing

In Figure 18 all of the results for two models are gathered and graphically presented. All data are achieved from the wing tip marked with white after set measurement to 0 for each angle of attack in zero freestream condition. According to the Figure 18, the displacement of the flexible wing tip is essentially linearly proportional to the angles of

attack in given conditions and such inclination is more prominent to deeper slope in higher velocity. This means that wing deformation due to the pressure distribution occurs to delay the separation on the wing in most velocity range for the MAV operation (20 *mph* to 50 *mph*).

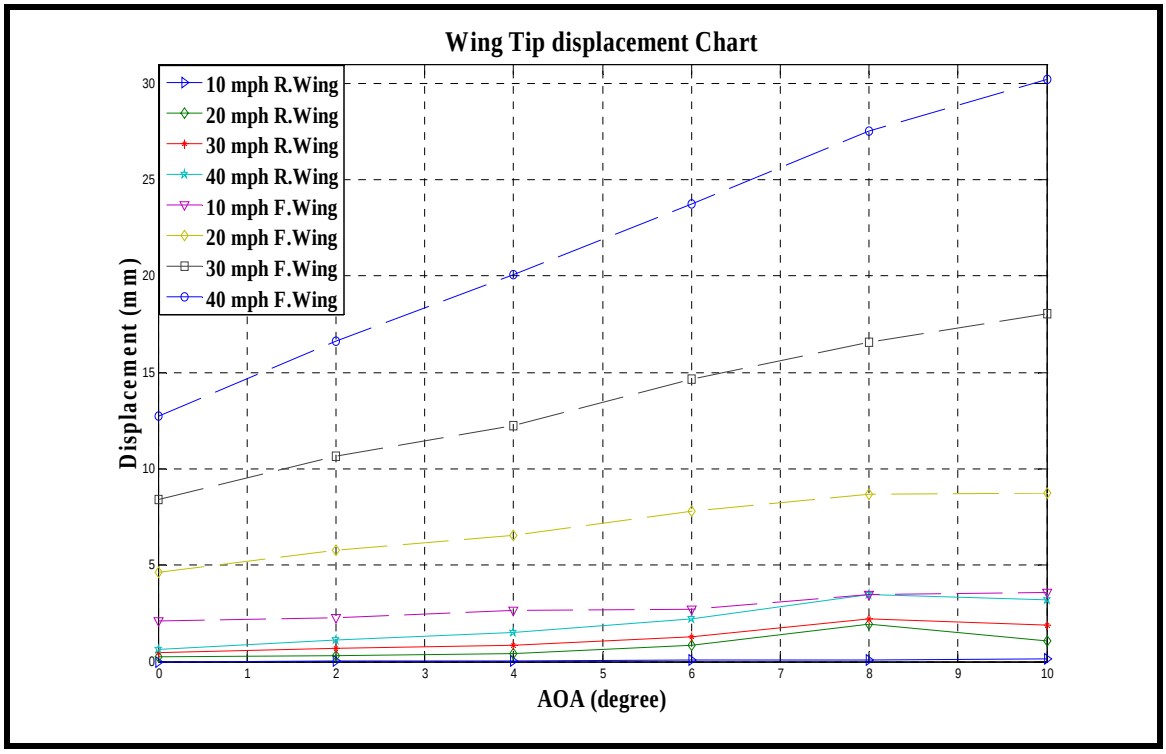

Figure 18. Wing Tip Displacement Chart for Rigid Wing & Flexible Wing in Z-direction

The displacement of the rigid wing is relatively smaller compared with the displacement of the flexible wing because the rigid wing has a stronger material stiffness than the flexible wing. In 10 *mph*, the displacement of the flexible wing is 2.5 - 3.5 times larger than that of the rigid wing, in 30 *mph*, 10 - 18 times measured and in 40 *mph*, 13 - 30 times. The rigid wing also has the proportional graph lines though the slopes are

relatively less steep than those of the flexible wing. This means that wing deformation occurs but the quantity of the wing deformation is small. It is noticeable that the slopes of the rigid wing is decreased at near the 8° angle of attack. This means that flow over the rigid wing is separated. Figure 19 shows the interaction of what take place on the rigid wing to cause the decrease of the slope of the displacement.

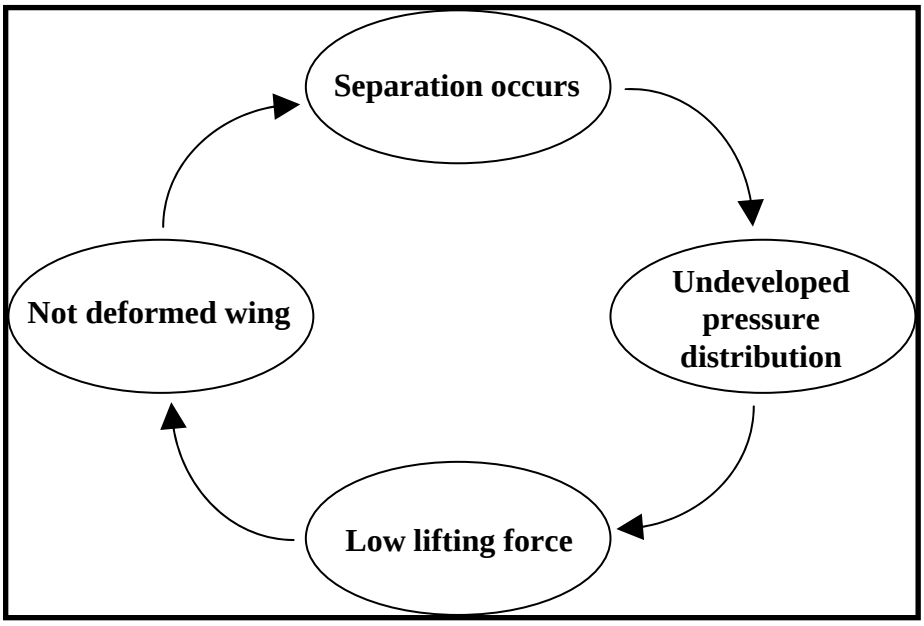

Figure 19. Interaction of Factors created on the Wing

According to the results of previous research for the MAV, the flexible wing provides the higher C_L and more reasonable L/D observed by Deluca et al. than rigid wing. It is proved that wing deformation based on the aeroelastic effect is related to the separation on the wing in this experiment. It is not generally the case that aeroelastic effects would offer a benefit.

Wing Tip Vortex system Results

The wing tip vortex system is considered as a combination of two components; axial-component (U_χ) and tangential-component (V_θ), in order to compare the vortex characteristics of two models in detail. For this experiment, velocity of 30*mph* was utilized as a freestream velocity in the wind tunnel. However, this freestream velocity was nominal. So, in order to reduce the error between the measured velocity and nominal velocity, all mean velocity are normalized by the average velocity of the tunnel freestream velocity achieved from an average of eight grid-points that was far away from the wing for each experiment. This value is denoted U'_∞ and is based on values measured by the hot-wire anemometer. So, Table 6 and Figure 20 show the results of the normalized axial velocity of the vortex core and to calculate the axial velocity, the maximum *u*-component value from the hot-wire data is utilized as an $U_{\chi,\max}$ for both models.

Model / AOA	Flexible ($U_{\chi,\max}/U_\infty$)	Rigid ($U_{\chi,\max}/U_\infty$)	Flexible ($U_{\chi,\max}/U'_\infty$)	Rigid ($U_{\chi,\max}/U'_\infty$)
0°	1.035	1.084	1.040	1.079
2°	1.163	1.099	1.154	1.085
4°	1.142	1.127	1.134	1.104
6°	1.132	1.118	1.121	1.091
8°	1.108	1.080	1.093	1.039
10°	1.070	1.088	1.052	1.041

Table 6. The Axial Velocity of the Vortex Core (U_∞ = 12.28 *m/s*)

To increase the objectivity, two notations, U_∞ and U'_∞, for the freestream velocity were utilized in above results. U_∞ is the freestream velocity from hot-wire probe at 0° angle of attack and this U_∞ is applied to all angle of attack as a freestream velocity. U'_∞ is the average velocity achieved from eight points where is the furthest from the vortex core in grids and this U'_∞ is recalculated whenever the angle of attack is changed. So, every angle of attack has different U'_∞ value. According to the results, the rigid wing has a higher value of $U_{\chi,\max}/U_\infty$ than flexible wing at 0° angle of attack. However, flexible wing has a considerably higher value than rigid wing at 2° angle of attack. That axial velocity of the vortex core is proportional to the strength of circulation (Γ) as stated in Chapter II. The flowfield for each type of wing exhibits the "jet-like" behavior described by Spalart (ref. 26) and others. The jet-like behavior has been reported to increase with angle of attack. The data acquired here did not show a steady increase in $U_{x,\max}$ for either wing. Rather the flexible wing exhibited a ten percent increase from 0° to 2° and a mild decline for larger angles. There was an increase in $U_{x,\max}$ for the rigid wing for from 0° to 4° and a subsequent decrease for larger angle of attack.

The same data can be presented in terms of Γ/Ub following the approach of Anderson E. A. and Lawton T. A. (ref. 2). Here Γ is calculated for the vehicles using Deluca's data and the Kutta-Joukosky theory.

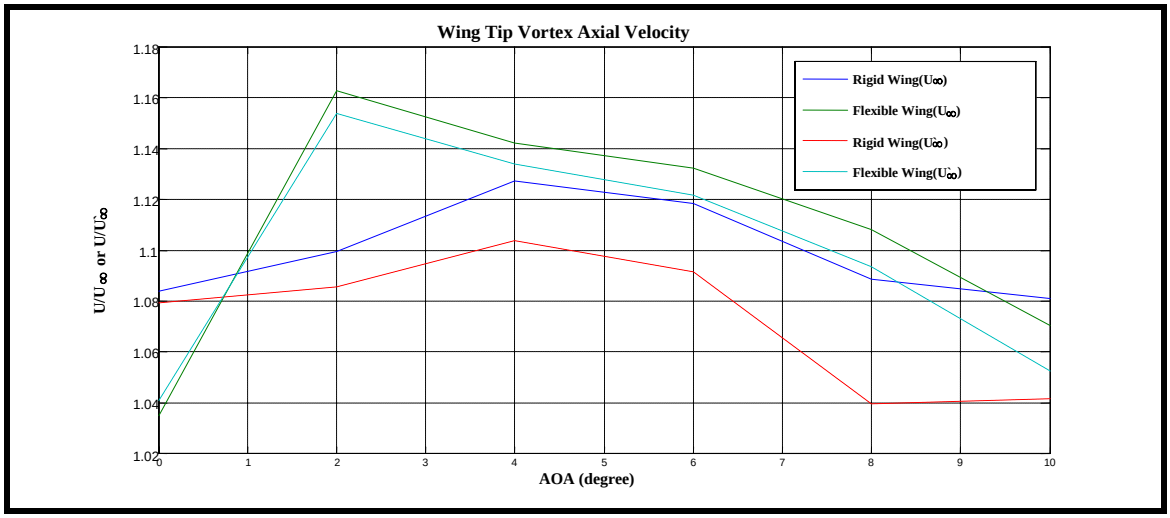

Figure 20. Axial Velocity as a Function of Angle of Attack

At 2° angle of attack, the flexible wing has maximum value after that has declined slope. The flexible wing entirely has a higher value than the rigid wing except for 0° and 10° angle of attack. However, when U'_{∞} is applied, the flexible wing has a slightly higher value than the rigid wing at 10° angle of attack due to the difference of between U_{∞} and U'_{∞}, which is likely a result of blockage. It is predictable that the rigid wing has higher value than the flexible wing right after 10° angle of attack, considering the slopes of two lines. On the other hand, rigid wing has high axial velocity at 4° angle of attack and overall axial velocity line has lower slope than flexible wing. It is notable that the rigid wing has higher axial velocity at 10° angle of attack. The comparison of two models related to the axial velocity of the vortex core is also presented with vortex plots in a later part.

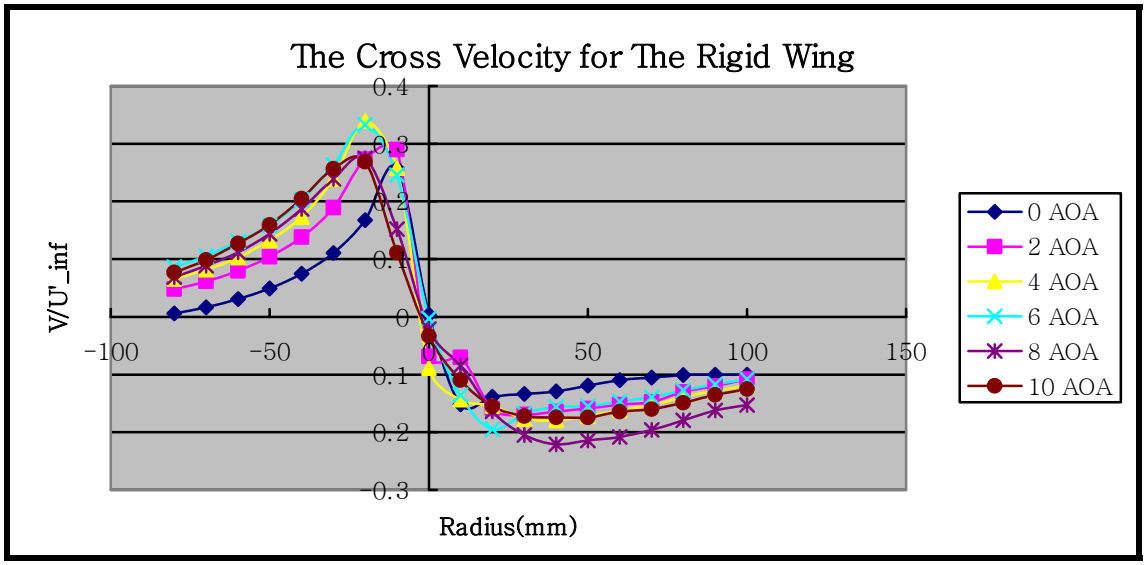

Figure 21. The Cross Velocity of the Vortex Core for the Rigid Wing

Figures 21 and 22 indicate the strength of the circulation by showing the v-component of velocity at the core of vortices as a function of angle of attack for two models. In these Figures, the cross velocity of the flexible wing is about 2 times the upper side of vortex core, at the lower side of the vortex, 1.5 times as larger as that of the rigid wing. This result indicates that the circulation about the tip vortex for the flexible wing is higher than on the rigid wing. It is notable that in both models, the peak value of the circulation at 10° angle of attack is almost the same or slightly lower than at 8° angle of attack due to increased wake turbulence based on the separation.

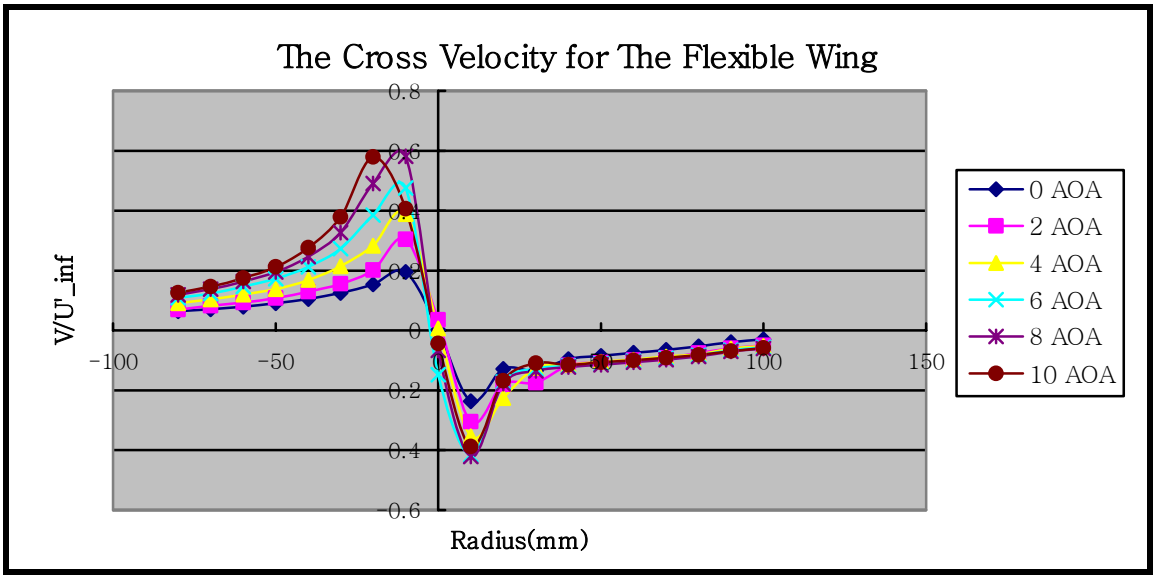

Figure 22. The Cross Velocity of the Vortex Core for the Flexible Wing

To calculate the cross velocity, the location of the vortex cores were directly found from the wing velocity contour maps in the following section and the hot-wire data matched with the location of the cores were utilized.

AOA \ Model	Flexible ($\sqrt{V^2+W^2}/U_\infty$)	Rigid ($\sqrt{V^2+W^2}/U_\infty$)
0°	0.396	0.376
2°	0.460	0.609
4°	0.515	0.508
6°	0.673	0.568
8°	0.588	0.482
10°	0.531	0.455

Table 7. Max Cross Velocity Magnitude of the Vortex

The table 7 and Figure 23 show the results of the calculation about tangential velocity. These results indicate that rigid wing has a peak value at 2° angle of attack and after this

point, rigid wing generally has a down-slope. But the flexible wing has a up-slope until 6° angle of attack and the peak value in the flexible wing is higher than in the rigid wing. This means that the flexible wing has a stronger magnitude of air circulation in high angle of attack than the rigid wing.

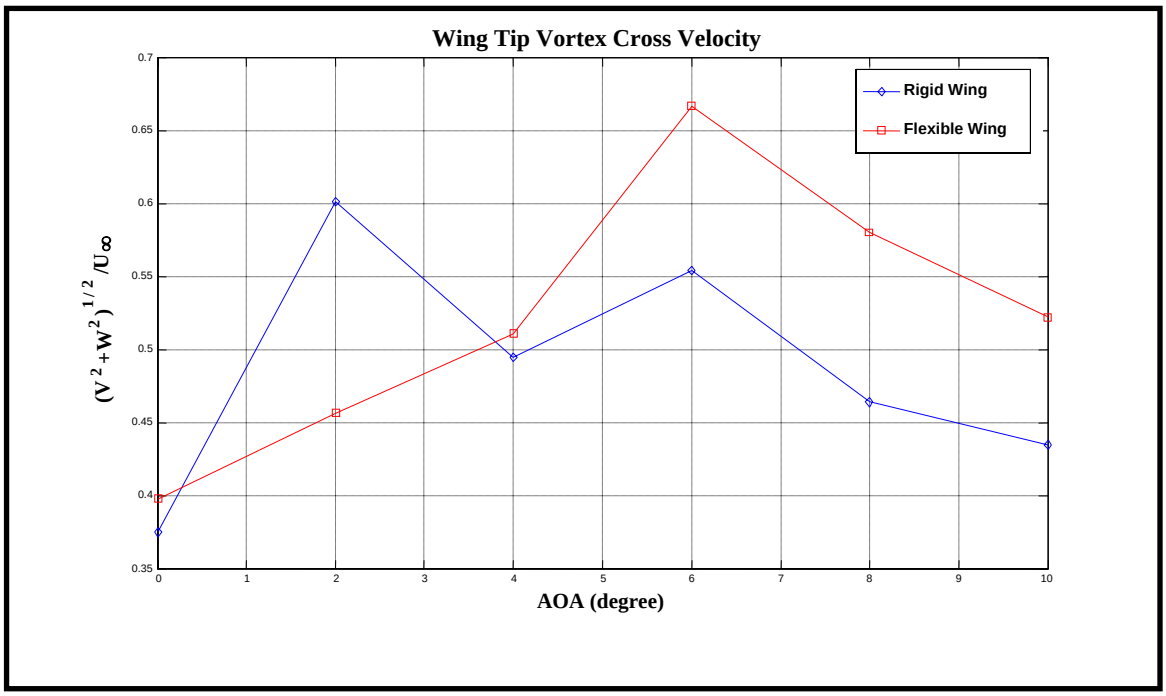

Figure 23. Cross Velocity Magnitude as a Function of Angle of Attack

In Figure 24, axial velocity is presented as a function of circulation parameter. To calculate axial velocity, nominal velocity was used as a freestream in this case. Figure 24 shows near the same inclination with Figure 20. As the circulation increases, axial velocity is increased in general. After around 8° angle of attack, the rigid wing and the flexible wing model have a decreased slope. Such result is not consistent with the general

cases. However, the result in Figure 24 can not be judged as a general inclination of these models because the range of the circulation parameter applied in this study is very narrow. Thus, it is said that Figure 24 shows not the entire inclination but partial inclination as a function of circulation parameter. Entire inclination should not be judged by Figure 24 and to find entire inclination of these models, wider range of circulation is needed.

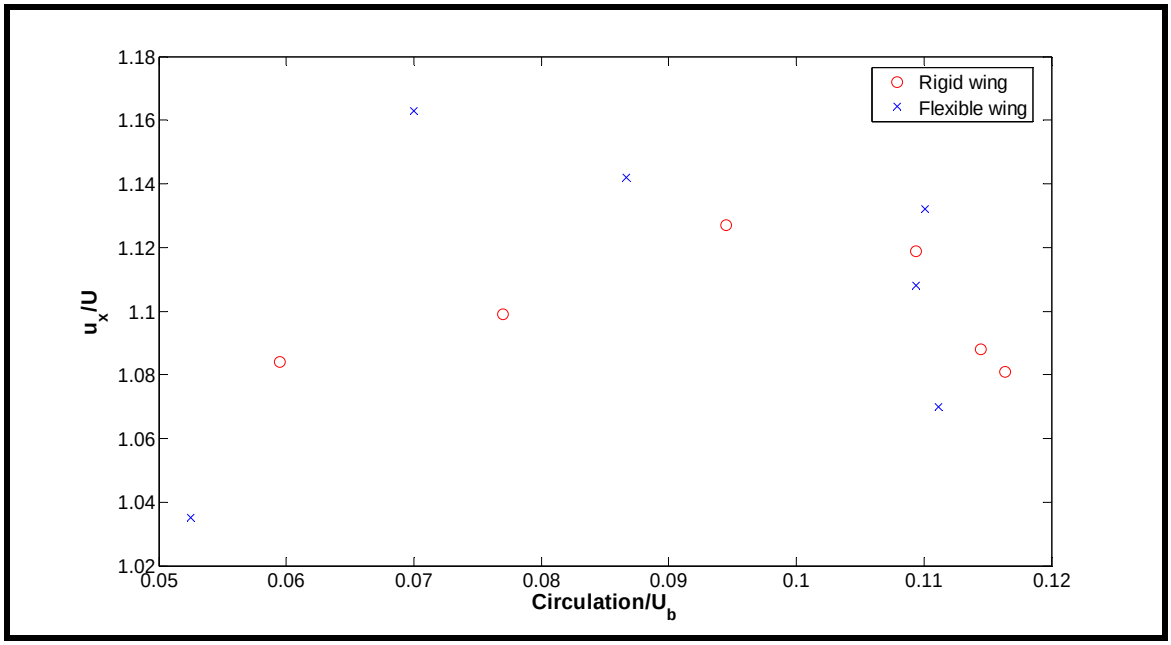

Figure 24. Axial velocity near the center of the vortex as a Function of Circulation Parameter

For the second part of the analysis, color contour maps of each of the different test are presented. In each of these plots, the point of view is looking at the MAV from behind as seen in Figure 17. All grids are presented as a function of angle of attack in *m/s*. On the contour plots, the color map represents the positive *u*-component. The black arrows indicate the v and w velocity acting in the cross-stream direction. Each legend shows a representative 1 *m/s* length vector. The *w*-component of the velocity acting in the *z*-

direction is slightly incorrect due to the imperfection in the mounting of the hot-wire probe. Since the end piece of the probe is so long, greater than 12 inches, it has a very slight downward angle to it that could not be physically overcome. It drops about 1/6" over the 12" length, which is only about 0.3°, but is enough to show a slight discrepancy in the *w*-component (B. Gamble, 2006:65). The contents referred above are in Figure 25.

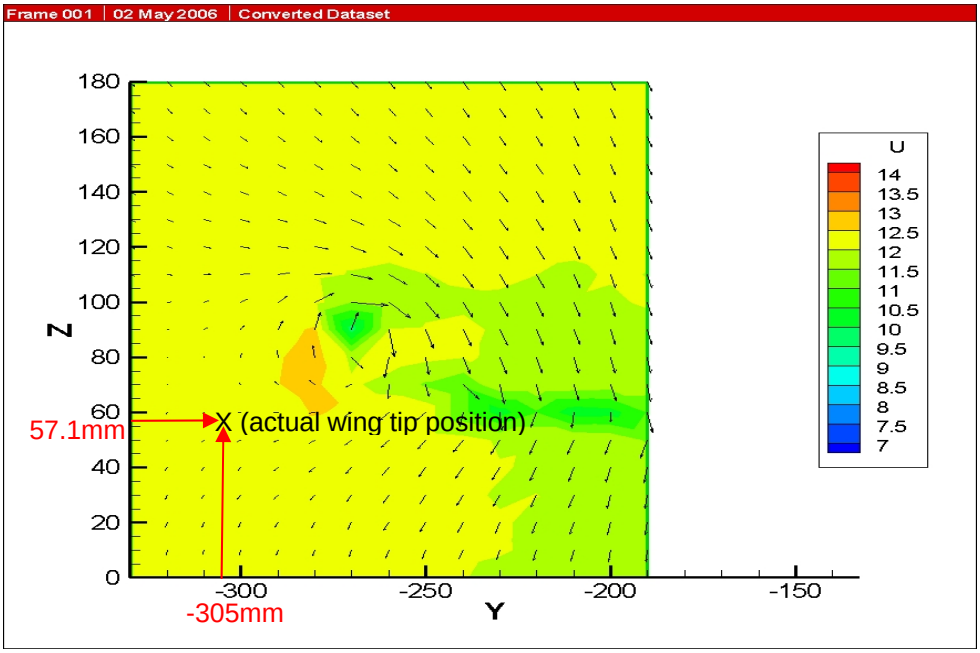

Figure 25. Velocity Profile of Left Wing Tip for Flexible Wing at 0° AOA

Center Wing Tail Velocity Profiles

The first set of plots shows the results of the velocity profiles on the center wing tail, grid 2 in Figure 17, between rigid wing and flexible wing. Contour lines are based on the *u*-component and black arrows show the *w*-component. To be objectively compared, the same legend is applied to all plots. Figure 26, 27, 28, 29 and 30 show velocity profiles

for center wing tail between two models. In Figure 26(α=2°), rigid wing has a little bit relatively lower velocity area (green color) than flexible wing. This means that the factor wake in this region is smaller on the flexible wing than on the rigid wing.

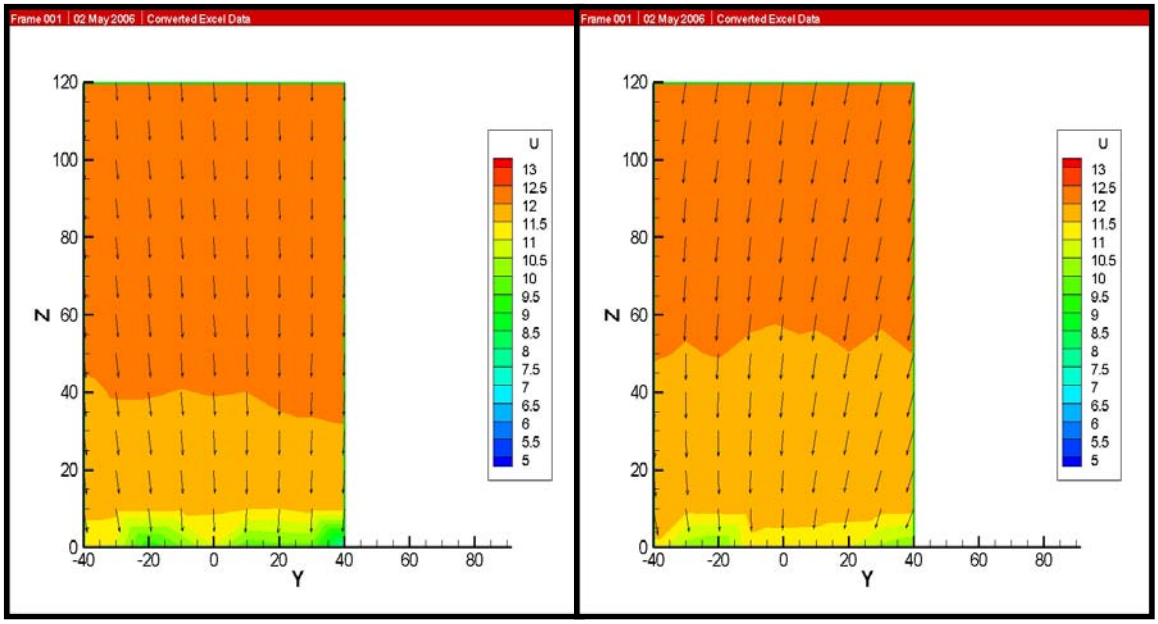

Figure 26. Velocity Profile of Center Wing Tail for Rigid (left) & Flexible (right) Wing at 2°AOA

With the increase of angle of attack, the low a velocity area is increased as seen in Figure 27 and the low velocity area of the rigid wing is more rapidly spread.

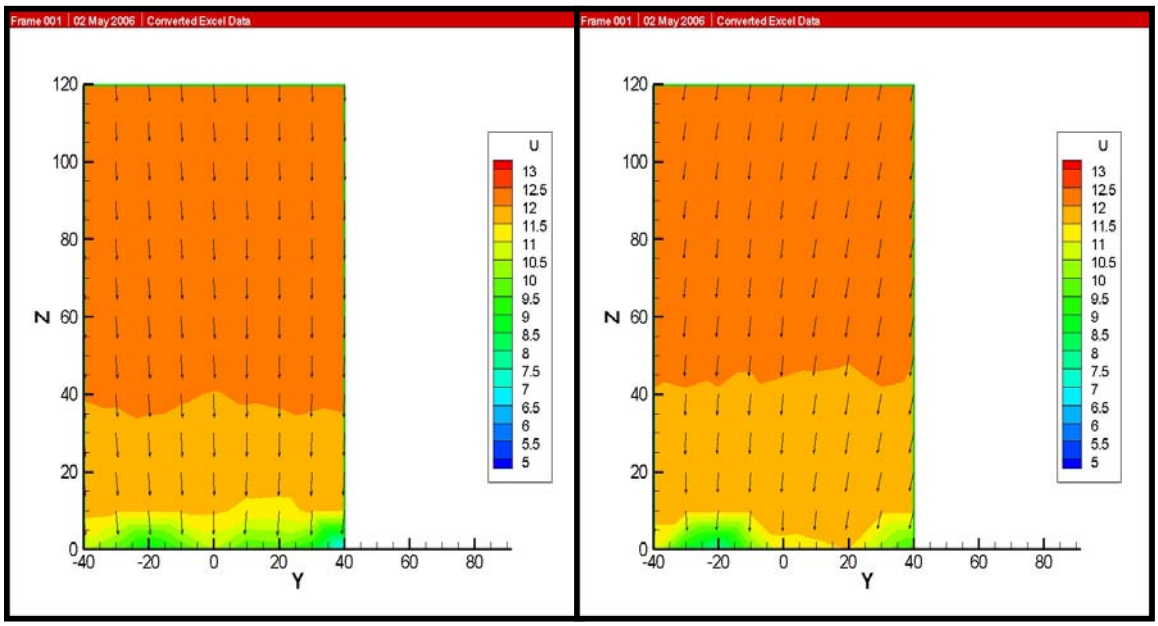

Figure 27. Velocity Profile of Center Wing Tail for Rigid & Flexible Wing at 4°AOA

Namely, it means that the expansion of the wake region according to the change of angle of attack is more radical than of the flexible wing. The middle part of the wing is directly attached to fuselage firmly. This inclination is also shown in Figure 28. In Figure 28, low velocity area is expanding and the rate of this expansion is faster in the rigid wing than in the flexible wing.

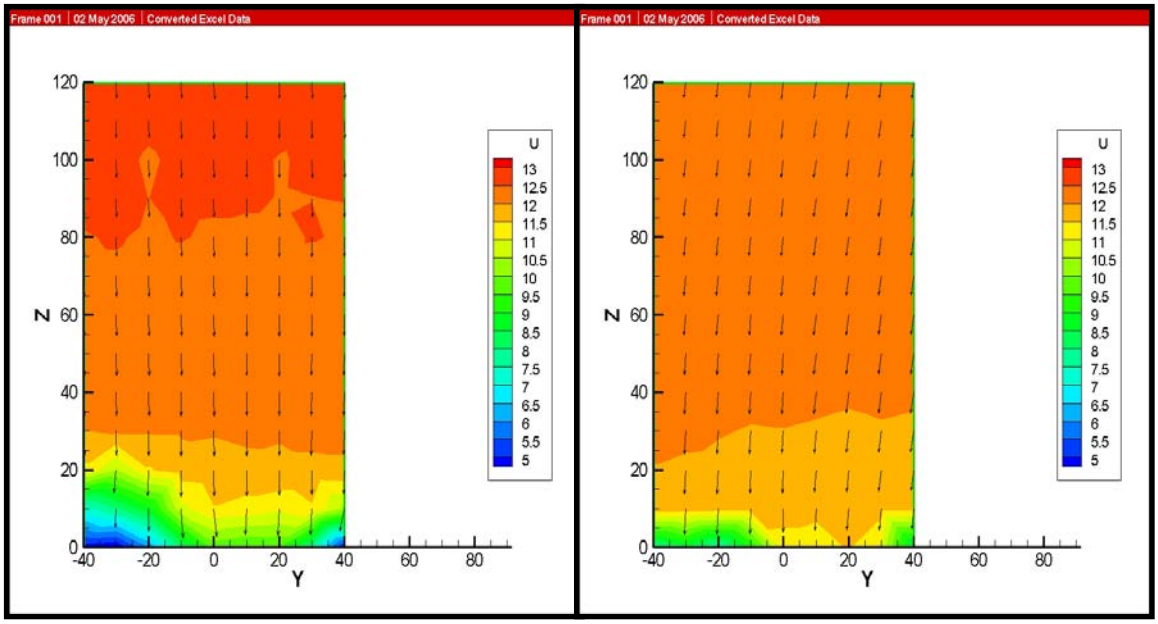

Figure 28. Velocity Profile of Center Wing Tail for Rigid & Flexible Wing at 6°AOA

In Figure 29 ($\alpha = 8^{\circ}$) and Figure 30 ($\alpha = 10^{\circ}$), the expansion of the wake is remarkably shown and the *w*-component of the rigid wing is also stronger than that of the flexible wing as seen in Figure 27.

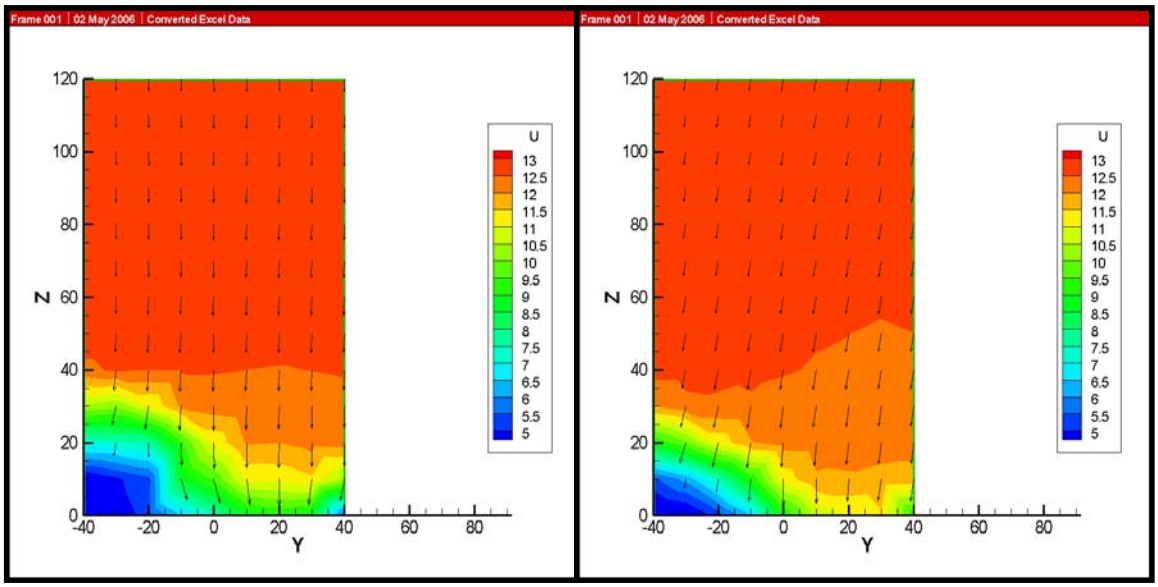

Figure 29. Velocity Profile of Center Wing Tail for Rigid & Flexible Wing at 8°AOA

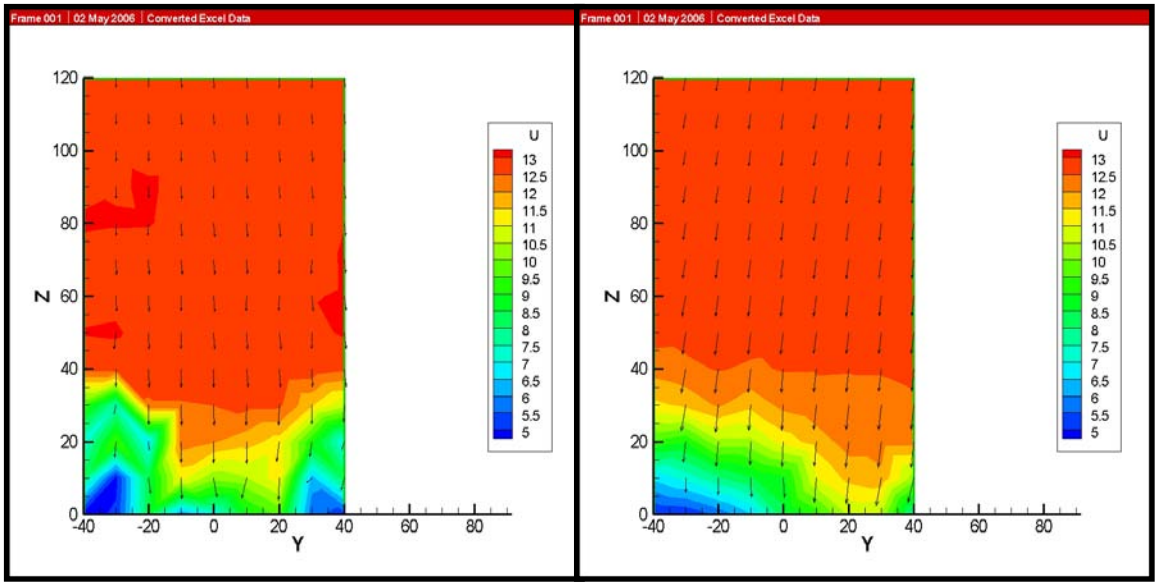

Figure 30. Velocity Profile of Center Wing Tail for Rigid & Flexible Wing at 10° AOA

In Figure 30, it is recognizable that the wake of the rigid wing is more irregular and spreads bigger space. Lastly, on the center wing tail area, it is proved that the flexible wing has faster and more stable u-component than the rigid wing through all angle of attack range.

Left Wing Velocity Profiles

Figures 31(α=2°), 32(α=4°), 33(α=6°), 34(α=8°) and 35(α=10°) show velocity profiles captured behind the left wing using grid 1. For the rigid wing, low velocity area is still greater than in flexible wing and has more unstable velocity distribution as seen in Figure 31. This plot shows the similar inclination with center wing tail velocity profile. However, plots show the *u*-component velocity profiles added the more vibration on the wing due to separation as the change of angle of attack.

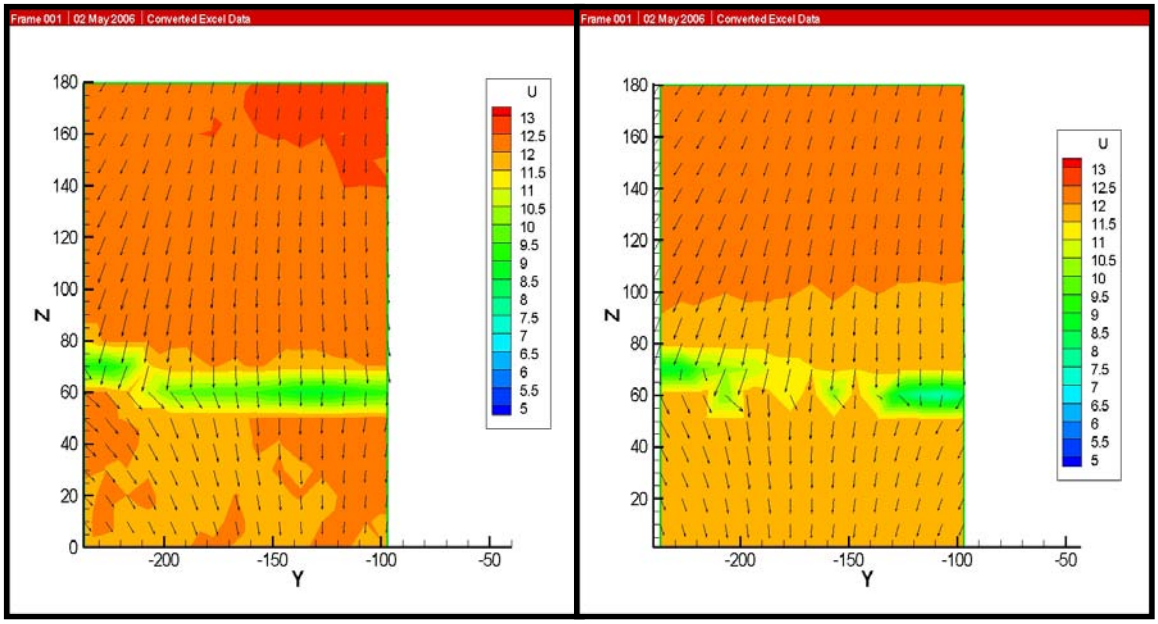

Figure 31. Velocity Profile of Left Wing for Rigid (left) & Flexible (right) Wing at 2° AOA

In Figure 31, the rigid wing has a larger low velocity region than the flexible wing. This plot shows different inclination with center wing tail plots because both wings take more influence from vibration based on separation. The shape of the wake of the wings in Figure 31 is described like a discontinued plane. The low velocity region grows bigger toward the wing tip. The wing tip was located at Y = -305 *mm* as represented on each plot. This inclination is demonstrated well in following plots. This indicates that the rigid wing produces wider wake disturbing the *u*-component velocity than the flexible wing.

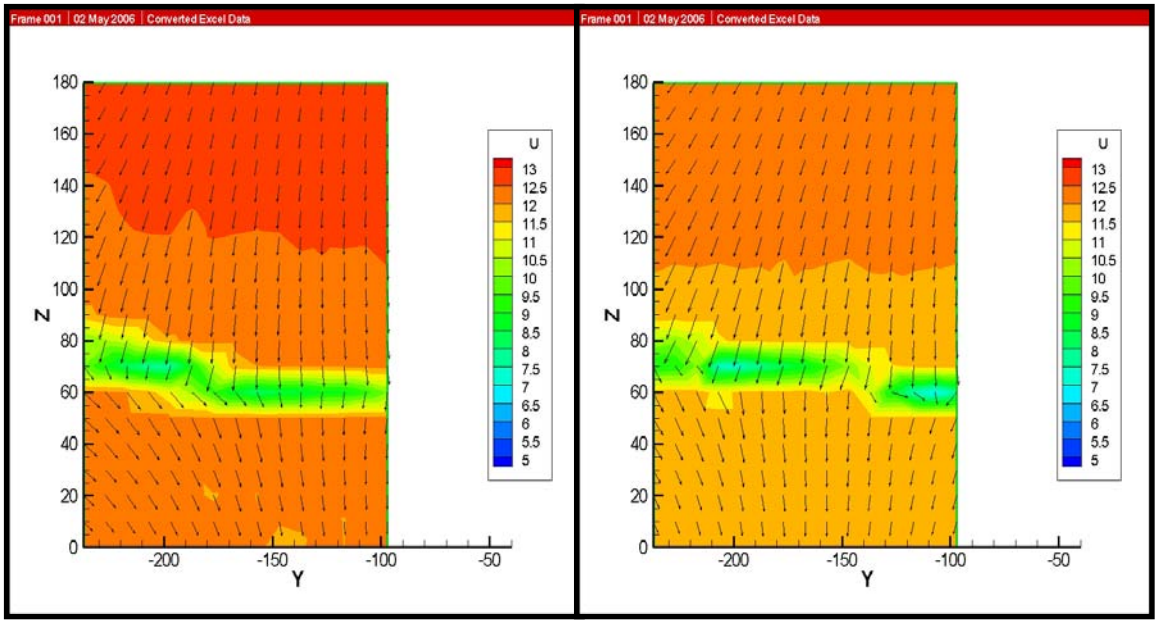

Figure 32. Velocity Profile of Left Wing for Rigid & Flexible Wing at 4° AOA

Thus, the flexible wing has a partially lower velocity area (blue color) is clearly shown in Figure 32 and Figure 33. From Figure 34, it is recognizable that the deficit in the u-component of velocity is larger for the rigid wing, which is consistent with a larger separation. As stated earlier, the flexible wing deforms due to aeroelastic effects, which allows the separation to be delayed. So, the flexible wing has a partial lower velocity area near the trailing edge. This means that freestream flows along with the flexible wing surface more for a while than the rigid wing. Therefore low velocity area appeared earlier in the flexible wing than in the rigid wing. This inclination is also demonstrated in high angle of attack contour plots.

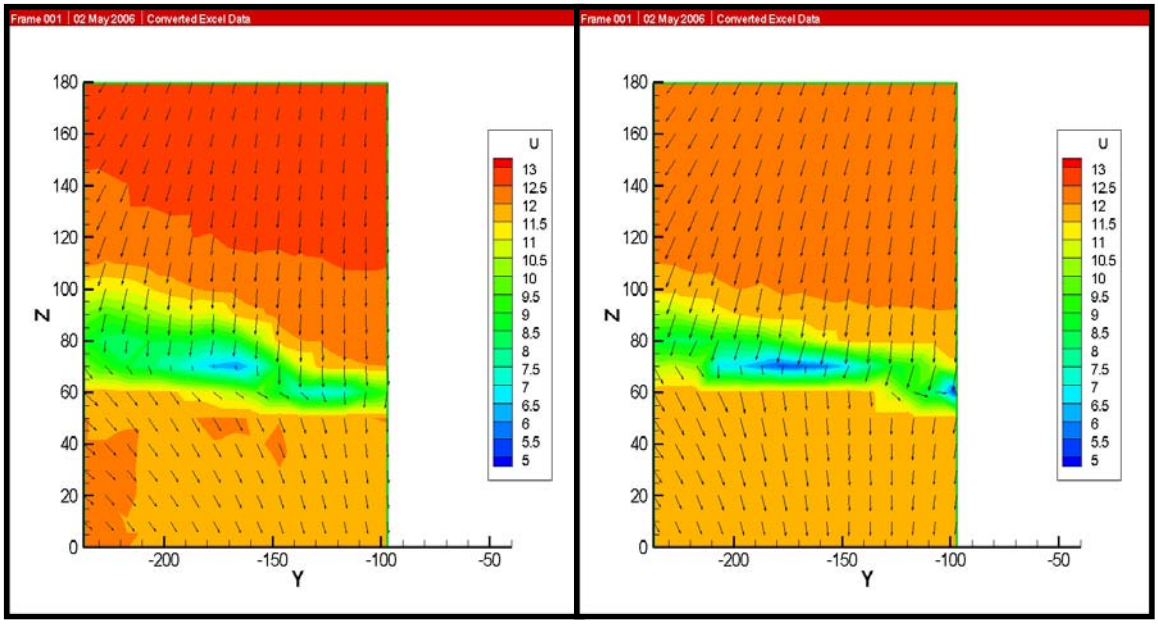

Figure 33. Velocity Profile of Left Wing for Rigid & Flexible Wing at 6° AOA

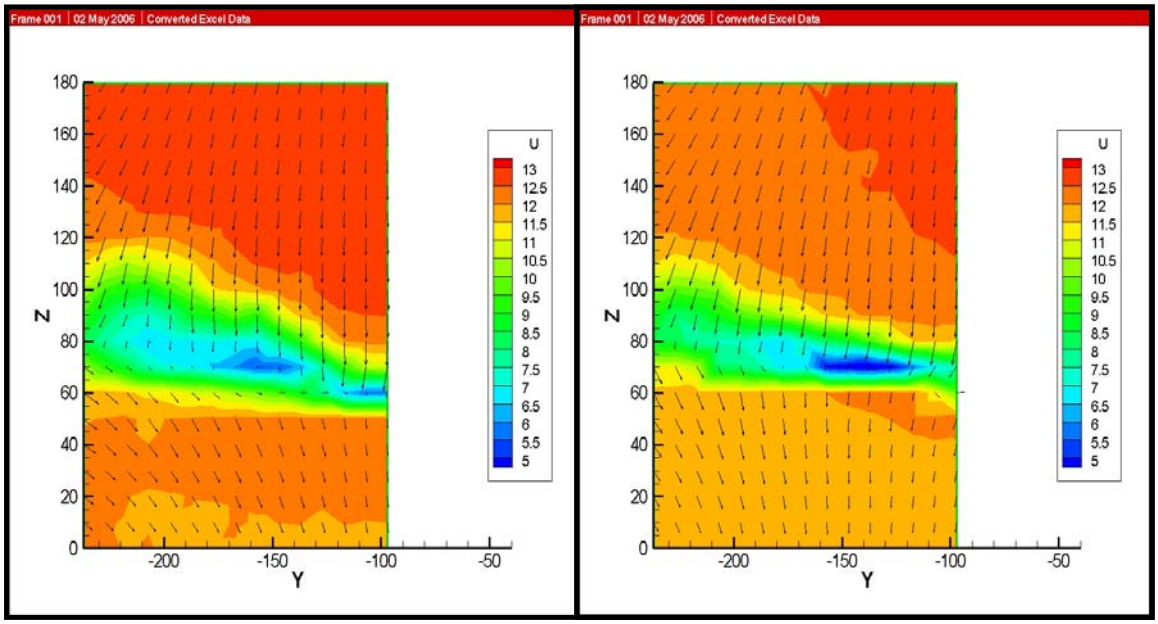

Figure 34. Velocity Profile of Left Wing for Rigid & Flexible Wing at 8° AOA

In high angle of attack with the same freestream velocity, the occurrence of separation comes to be gradually faster than before. Due to separation, the vibration generated on the wing is also intensified. Properly deformed wing due to the pressure distribution has the separation point delayed and due to the delayed separation, the vibration is generated less. Especially, this inclination is more clearly shown in high angle of attack as seen in Figure 35.

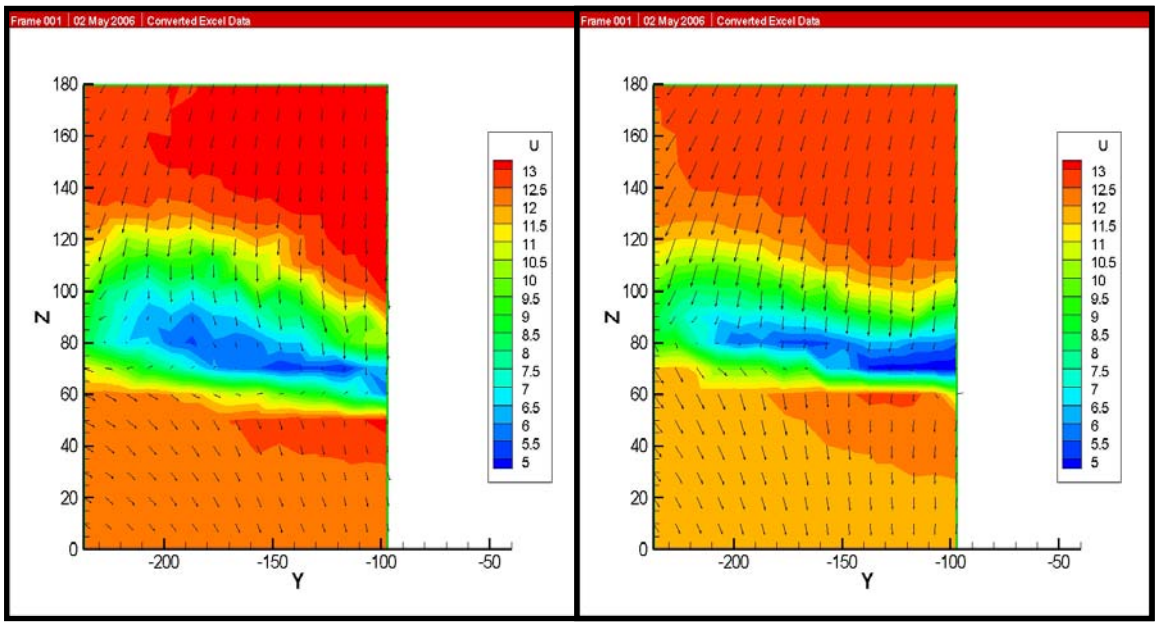

Figure 35. Velocity Profile of Left Wing for Rigid & Flexible Wing at 10° AOA

Left Wing Tip Velocity Profiles

In the previous section, aerodynamic differences on the wing between the rigid wing and the flexible wing were demonstrated with some pictures. The purpose of this section is to utilize the velocity profiles measured in the wind tunnel to analyze the wing tip vortices for two models. The velocity profiles in Figures 36, 37, 38 and 39 are

achieved from the same experimental conditions with previous experiments and plotted in terms of *u*-component velocity of freestream with wing tip grid, grid tip, to compare the vortices of two models. The results in Figure 20 are visualized with some contour maps in this section and it is helpful to understand the circulation, movements, and the strength of the vortices. After wing tip vortex contour maps, the variation contour maps in terms of *u*-component velocity are shown to demonstrate the vortices removed the effects generated around the wing.

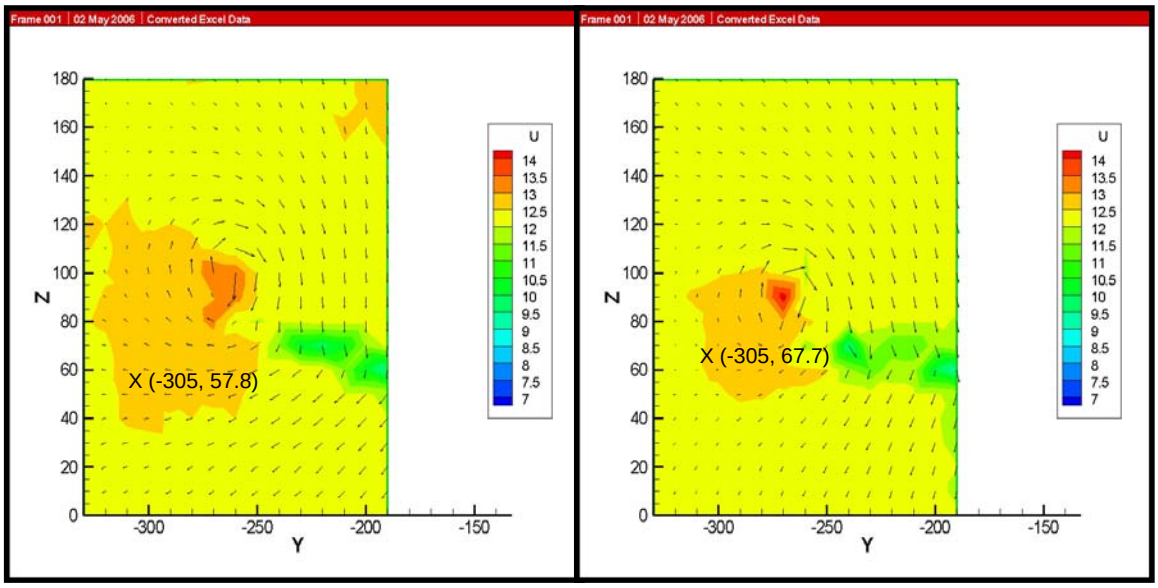

Figure 36. Velocity Profile of Left Wing Tip for Rigid & Flexible Wing at 2° AOA

In Figure 36, it is noticeable that in the same given conditions and 2° angle of attack, the flexible wing has more intensified and faster area (red area) and the axial velocity is directly proportional to the circulation. Also the region (orange area) influenced by wake turbulence is smaller on the flexible wing than on the rigid wing because the circulation

on the flexible wing tip is more concentrated and stronger due to delayed separation than on the rigid wing. In other words, the separation on the rigid wing tip occurs earlier than on the flexible wing tip. Therefore the vortices on the rigid wing tip do not enough have circulation to be intensified and strong.

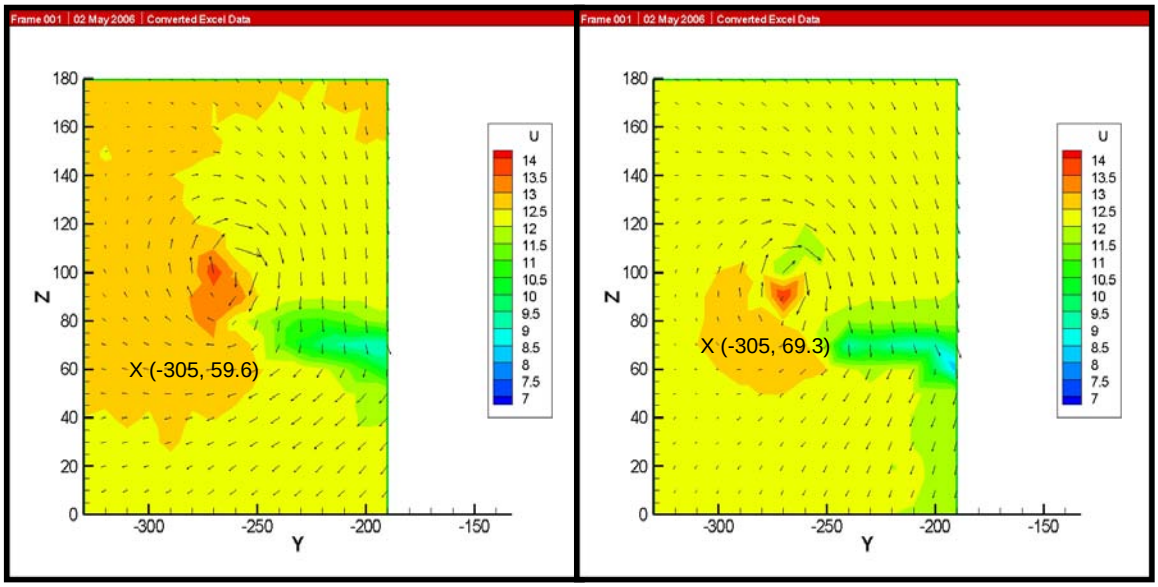

Figure 37. Velocity Profile of Left Wing Tip for Rigid & Flexible Wing at 4° AOA

The flexible wing has stronger circulation at the tip of the wing as seen in Figure 37. This means that the flexible wing has larger pressure difference between upper wing surface and lower wing surface. In Figure 38, the rigid wing plot shows more irregular axial velocity distribution than the flexible wing and the flexible wing still has faster area (red area) in the core of wing tip vortex at 6° angle of attack. These results demonstrated in previous contour plots coincide with the results in Figure 20. In Figure 38, the area (orange area) influenced by wake turbulence spreads more widely in the rigid wing

contour plot than in the flexible wing contour plot due to the effect of separation generated at the wing tip.

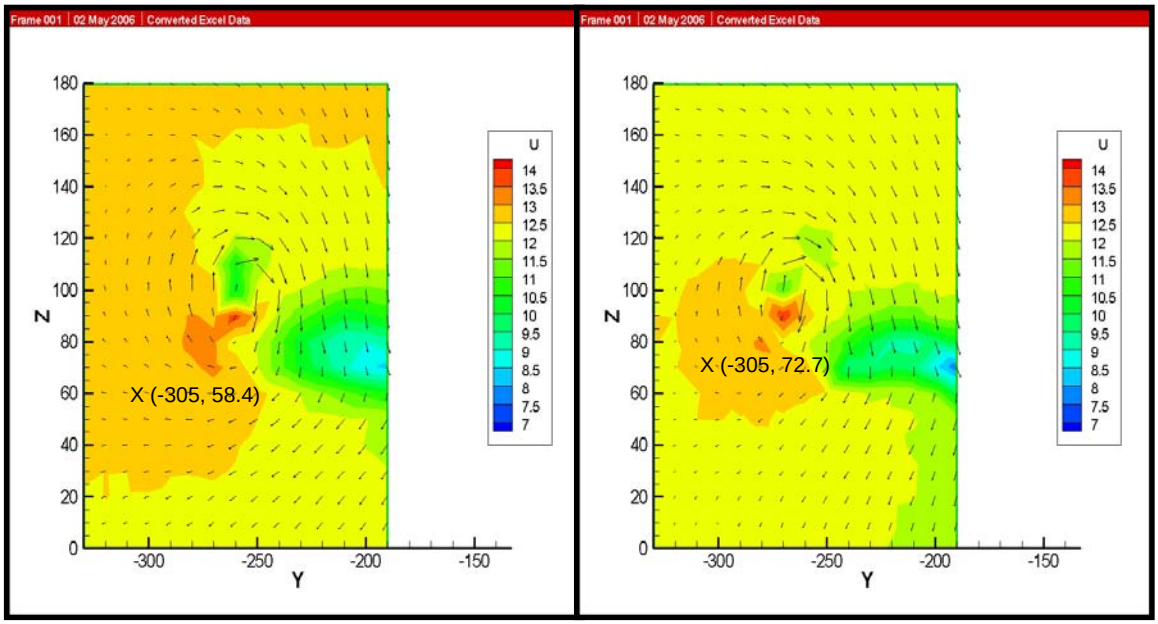

Figure 38. Velocity Profile of Left Wing Tip for Rigid & Flexible Wing at 6° AOA

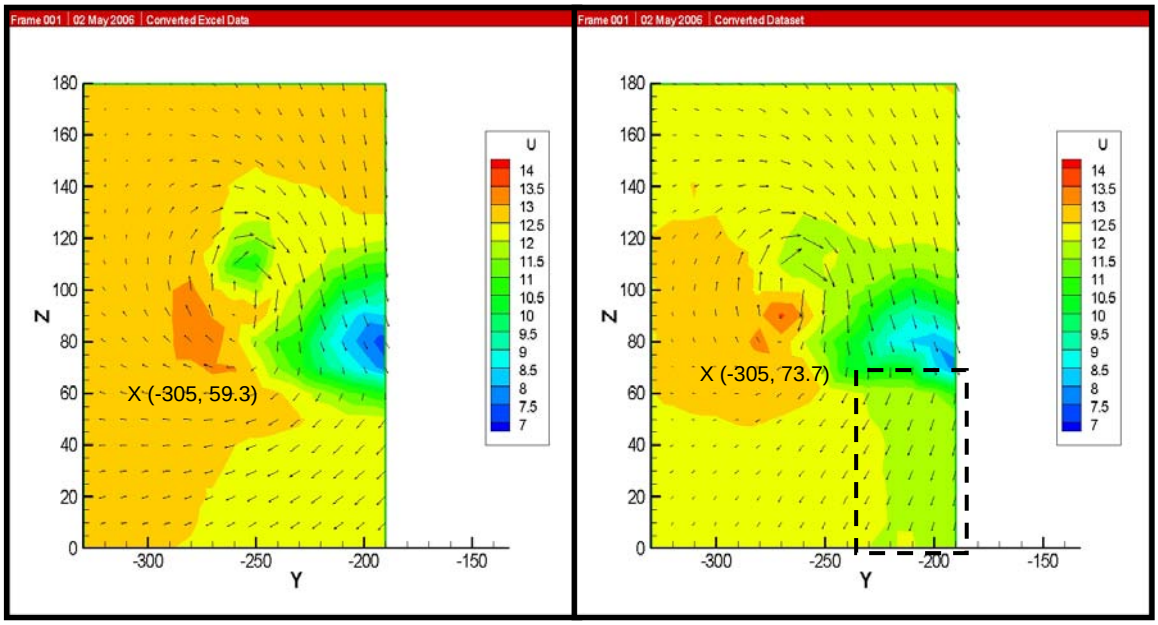

Figure 39. Velocity Profile of Left Wing Tip for Rigid & Flexible Wing at 8° AOA

In Figures 37 and 38, it is recognizable that the increase of the area influenced by wake turbulence in the flexible wing is considerably less than the rigid wing and according to Figure 39, the flexible wing has a unique area (black-dotted box) that the rigid wing has not. This proves that the *u*-component velocity of the freestream on the flexible wing is more disturbed by the downwash generated by delayed separation. That is, since the freestream flows for longer time on the flexible wing without separation than on the rigid wing, the flexible wing has relatively large downwash component. But the flow on the rigid wing has less influence from downwash due to separation. So, the downwash component generated on the flexible wing gives an influence to the *u*-component of the freestream.

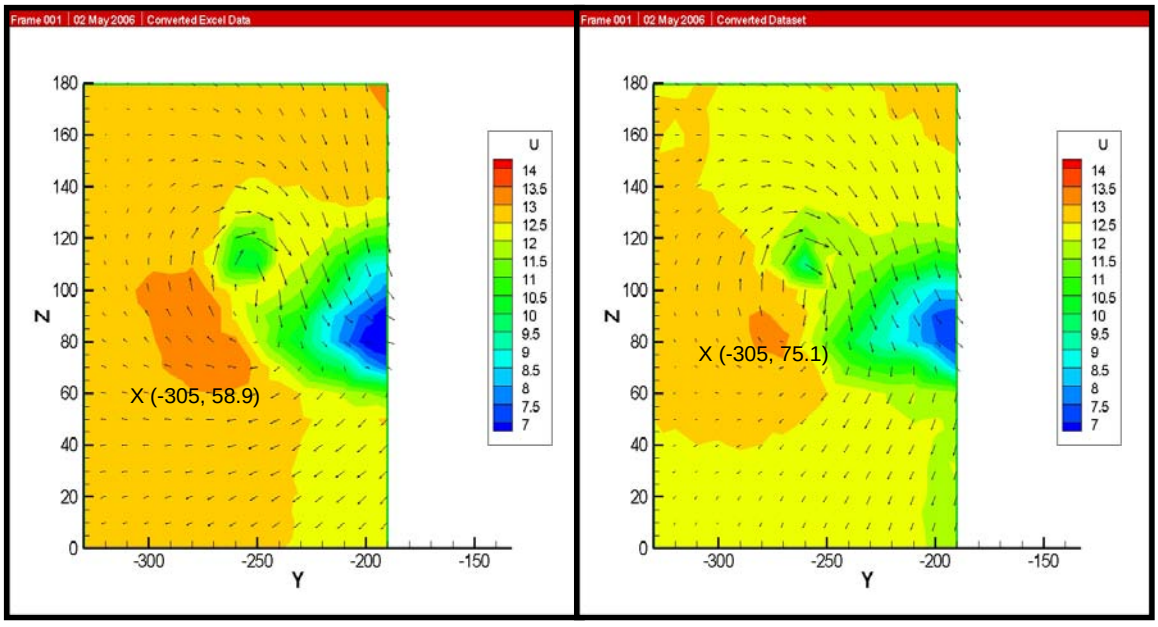

Figure 40. Velocity Profile of Left Wing Tip for Rigid & Flexible Wing at 10° AOA

Figure 40 shows that the axial velocity at the core has no higher value due to increased separation. This inclination is notably observed after 8° angle of attack according to Figures 21 and 22.

The Location of the Tip Vortex Core for the Flexible Wing

This section is devoted to investigating the location of the wing tip vortex and to demonstrate the characteristics of the flexible wing in detail. A finer grid was utilized in this investigation and this grid has the same size as the tip grid used in previous tests in Figure 17 but it has resolution of 2 times higher than previous tip grid. Except for the resolution, all conditions applied in this test are the same with the previous tests and this test performed with finer grid was conducted for the flexible wing model only. In Figure 41, 42and 43, the location of the wing tip vortex, the axial velocity and velocity distribution in the whole grid are demonstrated well. In Figure 41, the location of the vortex core is in the traverse coordinate of (-270, 90) at 0° angle of attack and in the coordinate of (-270, 95) at 2° angle of attack and the *u*-component of the freestream velocity is relatively increased at 2° angle of attack. The arrow vectors indicate that the circulation of the flexible wing tip is also increased at 2° angle of attack. In Figure 42, the location of the vortex core is in the coordinate of (-270, 100) at 4° angle of attack and (-270, 110) at 6° angle of attack and from 0° angle of attack to 6° angle of attack, the axial velocity is increased and the area (red area) is slightly expanded. Also the low *u*-component velocity area (blue area) at right above of the maximum axial velocity is

intensified. This means that the circulation is intensified as the angle of attack increases. This inclination is extended to 8° angle of attack. In Figure 43, the location of the vortex core is in the coordinate of (-265, 110) at 8° angle of attack and (-265, 115) at 10° angle of attack. In spanning from 0° to 10° the physical location of the wing tip is increased by 16mm. Furthermore, at 30 *mph*, wing tip flexure was 18mm. This accounted for 34mm. The vertical location of the peak velocity in the core is increased by only 25mm by comparison.

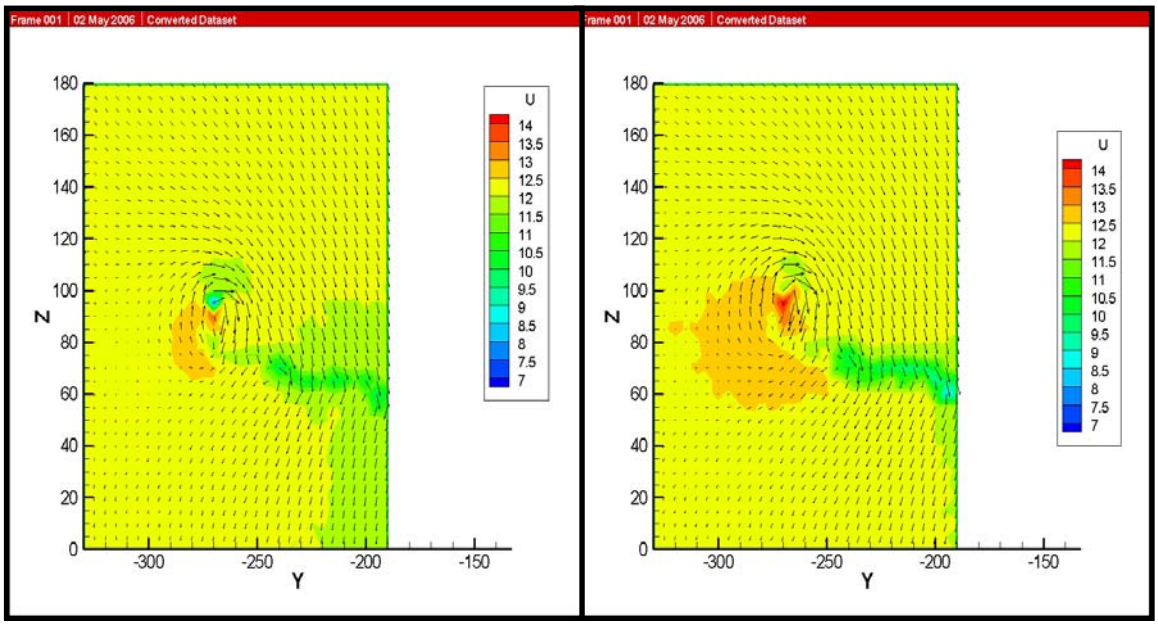

Figure 41. Finer Velocity Profile of Left Wing Tip for Flexible Wing at 0° & 2° AOA

It is note that these figures are plotted with the measured flow velocity. Therefore, actual wing and wing tip position can not be designated in these figures and the wing and wing tip position can not be calculated with the data. To match the wing and wing position to these figures, additional study is needed.

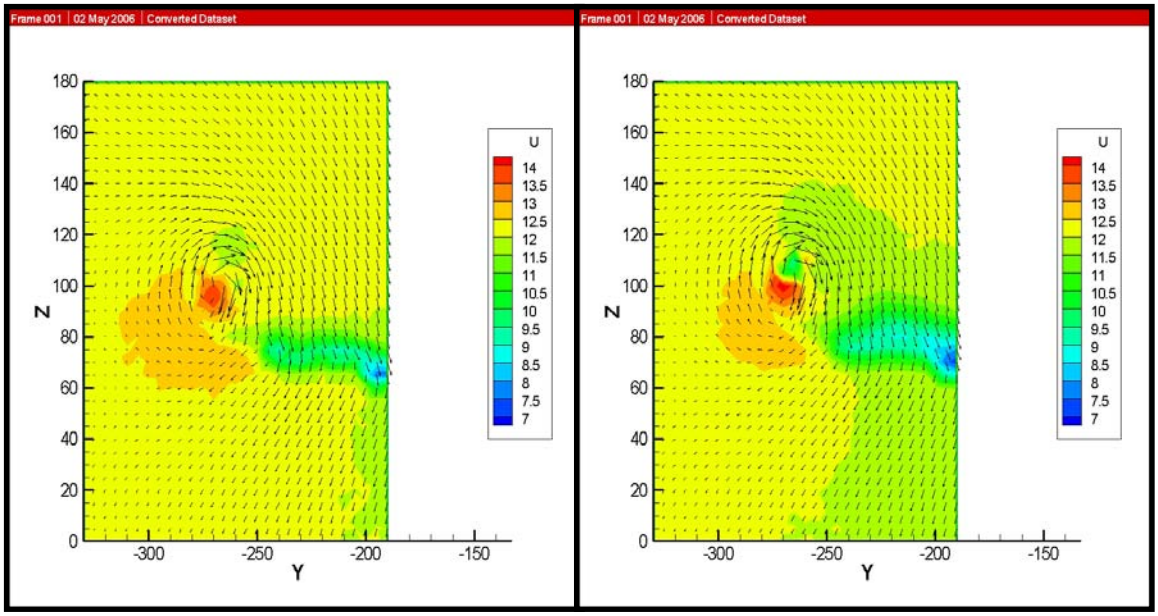

Figure 42. Finer Velocity Profile of Left Wing Tip for Flexible Wing at 4° & 6° AOA

Through the all range of angle of attack applied in this test, it is clearly proved that the location of the vortex core is ascended above the wing at 1" downstream of the wing. R. Spalart described the location of the vortex core in his study effort (ref. 25), as follows.

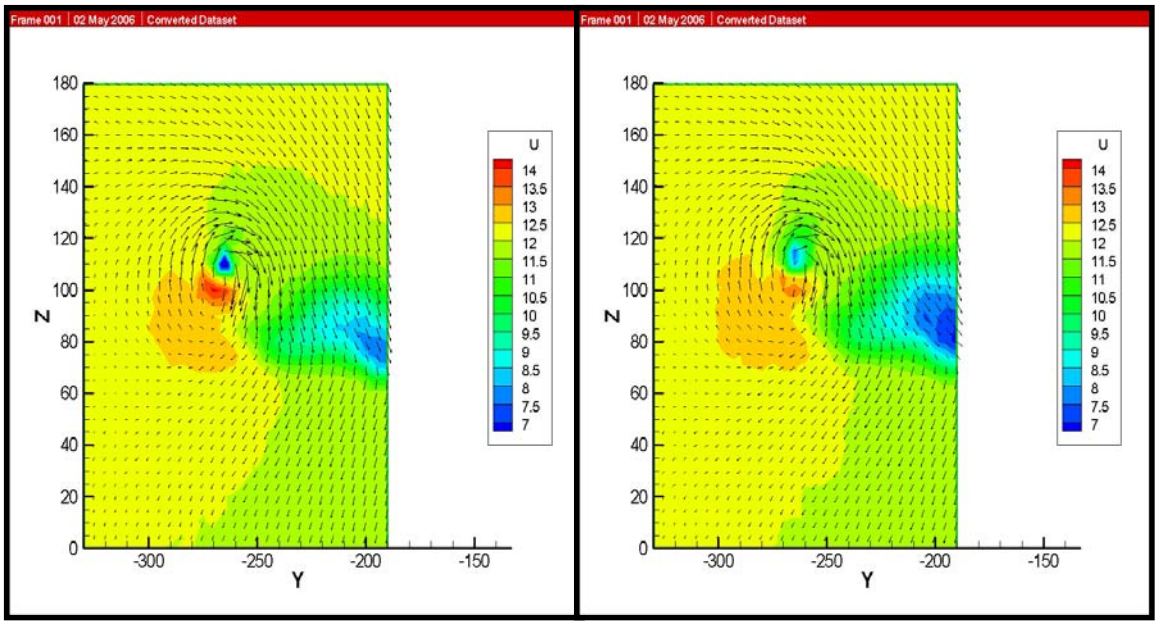

Figure 43. Finer Velocity Profile of Left Wing Tip for Flexible Wing at 8° & 10° AOA

"I now turn to a misunderstanding that remains common, regarding the initial behavior of the vortex sheet. Consider the two-dimensional (2D) sheet created by an elliptical circulation distribution: $\Gamma(y) = \Gamma_0(1-4y^2/b^2)^{0.5}$, if $|y| \le b/2$, and 0 otherwise. Initially the vertical velocity component *w* at the vortex sheet equals $w_0 = -\Gamma_0/b$ for $|y| < b/2$. This is the classical "uniform downwash" of lifting-line theory. Some authors then expect the exact sheet to descend, without deformation, at the rate w_0. 'Real' sheets would roll up because of "imperfections" at the tip or an "instability." This is incorrect, as shown most simply by Spreiter & Sacks (1951) (the velocity field is singular as $|y| \to b/2$, making elementary arguments elusive). Spreiter & Sacks derive the velocity of the centroid of vorticity from an integral that is insensitive to the tip singularity. That velocity equals $w_1 = -(1-\pi/4)\Gamma_0/b$, which is much smaller than w_0. Therefore, all the vorticity cannot be descending at w_0. At early times the central part of the sheet does descend at w_0, but its tips move upwards, initially at an infinite velocity. Rapid upward motion of the tip vortex is seen in actual three-dimensional (3D) wakes." (R. Spalart, 1998:115)

The results regarding the location of the vortex core in this study support the suggestion of R. Spalart. In Figure 43, the maximum axial velocity is radically decreased at 10° angle of attack because of wake turbulence generated at high angle of attack.

Left Wing Tip Turbulent Velocity Profiles

In Figures 44 and 45 the fluctuating velocity component (U') contour maps are utilized to help understand the relative velocity at the vortex core. The *u*-component of

the freestream is shown as a theoretically zero velocity (blue area) to focus to only the change of the *u*-component of the freestream along with the wings and these variation contour maps are helpful to recognize the typical shape of the tip vortex. In ref. 22, Mathieu J. and Scott J. defined the fluid velocity as $U_i = \overline{U_i} + u_i$, where U_i is the fluid velocity, $\overline{U_i}$ is the ensemble average velocity and u_i is the fluctuation, usually identified with the turbulence. In following turbulent velocity plots, only u_i-component is concerned and calculated to compare the turbulent state behind the models. Figure 44 clearly shows that the flexible wing has not only higher axial velocity but also higher circulation. In Figure 44, the axial velocity of the rigid wing is graphically higher than the flexible wing. It is slightly different result from the result in Figure 37. The error between two different results could come from the translation system transferring the collected electrical signal of hot-wire probe to the software connected with hot-wire probe. However, the software built in hot-wire anemometer system was not analyzed in this study. However, considering the axial velocity data, the cross velocity data and the wing tip velocity profiles, it is reliable

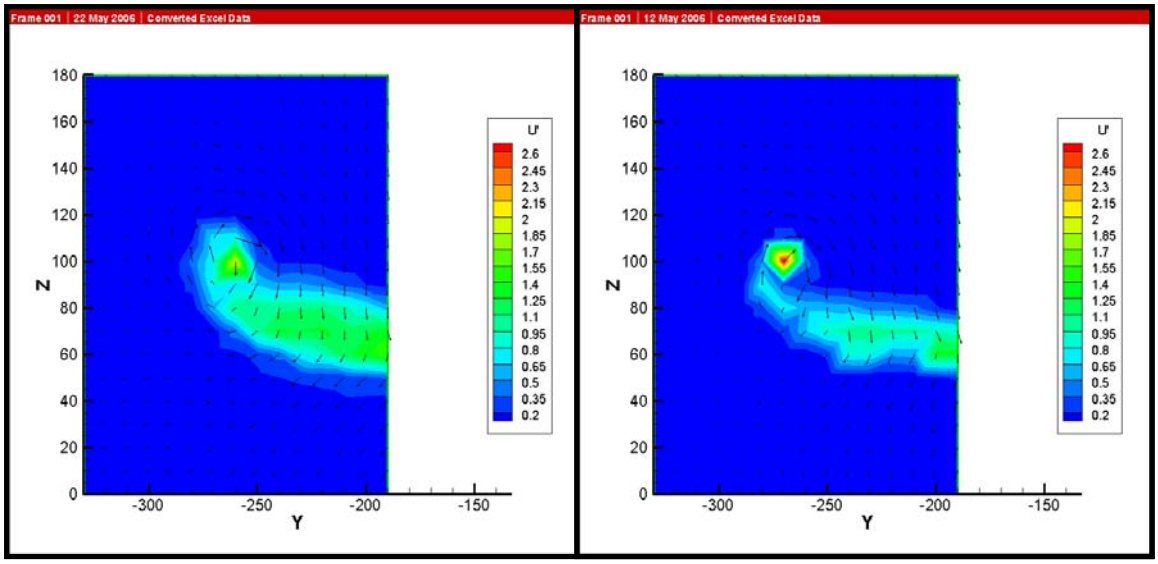

Figure 44. Variation Velocity Profile of Wing Tip for the Rigid Wing & Flexible Wing at 4° AOA

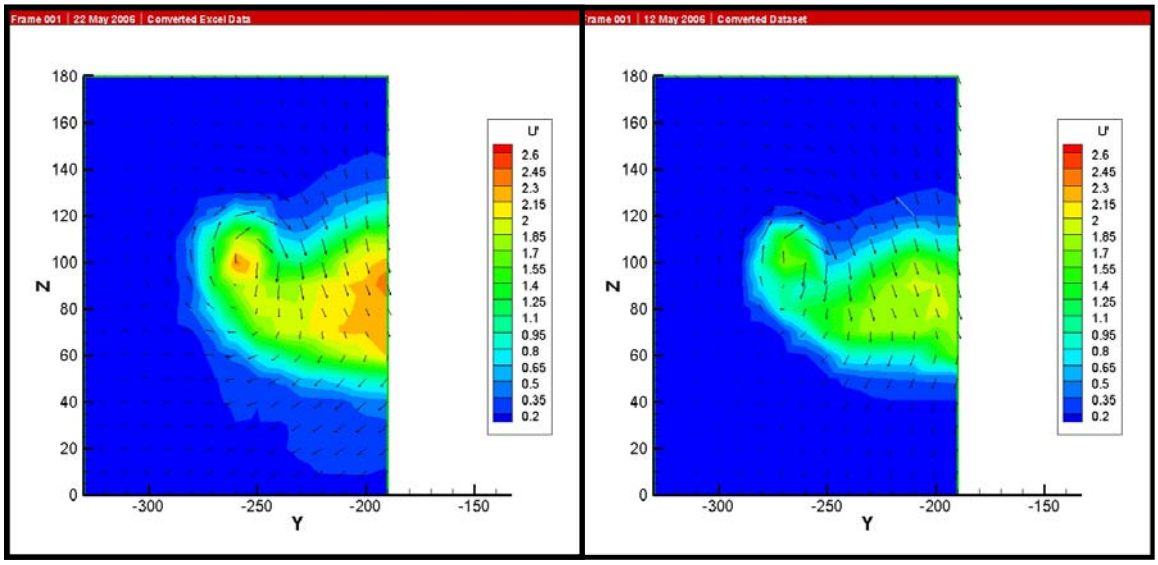

Figure 45. Variation Velocity Profile of Wing Tip for the Rigid Wing & Flexible Wing at 8° AOA

that the axial velocity of the flexible wing is still higher than of the rigid wing at 8° angle of attack. In Figure 45, since the separation generated on the rigid wing appeared earlier than on the flexible wing, the rigid wing has higher fluctuating velocity near the wing

surface than the flexible wing. That is, the freestream on the flexible wing is flows longer time without separation than on the rigid wing. Therefore, the freestream on the flexible wing has downwash factor and reduced *u*-component of the turbulent velocity.

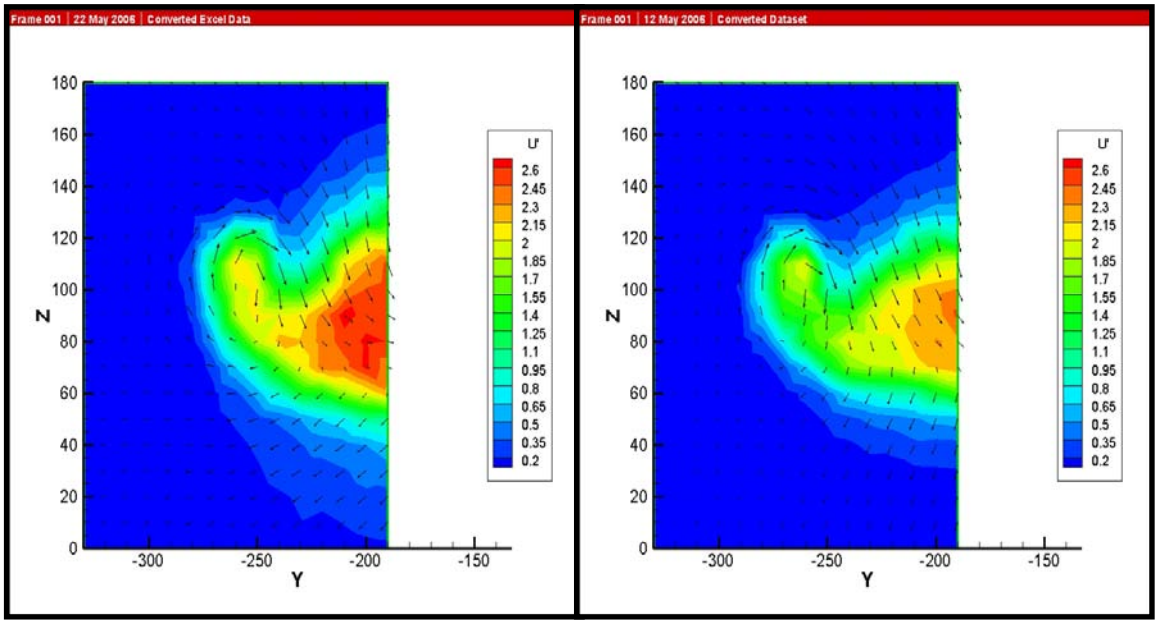

Figure 46. Variation Velocity Profile of Wing Tip for the Rigid Wing & Flexible Wing at 10° AOA

Summary

All of the tests conducted in this research can be used to justify wing efficiency for the MAV. From the wing tip displacement study, results indicate that adequate wing deformation is helpful to increase the wing efficiency until the wing begins to lose natural aerodynamic characteristics due to over-deformation. Velocity profile results from the wind tunnel tests provide insight into the separation and stall effects on both the flexible and rigid wings. Velocity profiles show how different flowfield is formed on the rigid

wing and flexible wing. Velocity profiles also show how different axial velocity is formed at the wing tip vortex. The cross velocity formed near the vortex core is demonstrated and the difference of the vortex core location is shown for both the rigid wing and flexible wing. Differences between the flexible and rigid wings are evident in the fluctuating velocity component profiles. Primarily, hot-wire data acquired from the wing tip displacement test indicated the flexible wing has better wing efficiency than the rigid wing due to wing deformation until high angle of attack. The velocity profiles also provided the flexible wing has higher axial velocity than the rigid wing. That is, the flexible wing also has higher cross velocity due to high pressure distribution based on aeroelastic effects and the rigid wing has larger low velocity area in all angle of attack applied in this study.

V. Conclusions and Recommendations

Overview

The main conclusions developed during the research of the wing tip displacement, wing tip vortex study on the MAV are presented in this chapter. The results of the tests show that the research effort successfully accomplished the purpose set forth set forth in Chapter I. Future recommendations for follow-on research, test improvements, and MAV design are included in an effort to expand upon the research conducted herein.

Conclusions and Significance of Research

This research closely examined that the wing displacement in terms of angle of attack and wing tip vortex system has on a micro-air-vehicle equipped with either a rigid or flexible wing. By developing a test setup that was able to measure optically the change of the wing tip displacement, the changes of wing as the change of angle of attack were investigated in detail for each MAV. This provided the opportunity to investigate the efficiency of between the rigid wing and the flexible wing. By testing the wing at various angles of attack, the efficiency of each wing was examined and wing tip vortex system was investigated. To investigate the wing tip vortex system for two models in detail, the axial velocity data, cross velocity, the location of the wing tip vortex core and variation data in terms of u-component of velocity were utilized. In these days, to increase the survivability and accuracy, important missions are performed by formational MAV group consisting of more than 2 sets. The research of vortex system provides the

essential information to determine the aerodynamic influence of wing tip vortex. Results from this test led to the following conclusions:

- The value of the flexible wing tip displacement is 3 – 7 times of the value of the rigid wing tip displacement in low freestream velocity (10 *mph* – 20 *mph*) and 10 – 30 times of the value of the rigid wing tip displacement in high freestream velocity (30 *mph* – 40 *mph*).

- The slope of the rigid wing tip displacement is radically decreased after 8° angle of attack due to separation. Whereas, the slope of the flexible wing displacement is increased in all applied angle of attack due to delayed separation based on the wing deformation.

- The flexible wing has less stall effects than the rigid wing until 8° angle of attack. But after 8° angle of attack, the flexible wing is losing own aerodynamic properties due to critical wing deformation. Wing deformation based on aeroelastic effect help increase the wing efficiency until reaching high angle of attack.

- The axial velocity in vortex system for both models is always higher than applied freestream velocity ($U_\chi/U_\infty > 1$) in all applied angle of attack. As the maximum axial velocity, the U_χ/U_∞ of the flexible wing is 1.16 or 1.15 and the U_χ/U_∞ of the rigid wing is 1.15 or 1.10. These results indicate that the axial velocity of the flexible wing is between 4.3% and 5% higher than that of the rigid wing for the conditions tested, which are representative of typical flight conditions.

- The cross velocity of the flexible wing at the vortex core is between 10% and 18% higher than that of the rigid wing for equal angle of attack.

- The location of the vortex core is ascended above the wing at 1” aft of the wing for both models. This result is consistent with the result of literature regarding the vortex system. The location of the vortex core of the flexible wing is between 5.5% and 15% higher than that of the rigid wing, due to wing flexure.

- Velocity profiles show that separation occurs on the rigid wing earlier than on the flexible wing and the rigid wing has a larger low velocity area than the flexible wing when approaching stall. However, the lowest velocity area exists in the flexible wing area due to downwash based on delayed separation.

- According to entire velocity profiles, the flexible wing has higher efficiency than the rigid wing until reaching 10° angle of attack in terms of separation, low velocity area, circulation and wing tip deformation.

The research conducted during this thesis provided many interesting and significant results. The differences in wing tip displacement and wing vortex system between a rigid and flexible wing MAV were successfully investigated for various freestream velocity and angle of attack. The use of multiple MAV's formation may be affected by the trailing vortex system, and it is important to have an understanding of the flowfield. These results and data could be used in the future to develop other MAV designs. Also it is very important that what material should be applied to meet the suggested requirements. The wing tip displacement data could be utilized to determine the adequate wing material and the telescopic survey tool developed in future could be a proper device to investigate the wing displacement. The patterns of the vortex core displacement could be could be utilized to examine the potential advantages to obtaining the clearance between the MAV and the MAV during operation. Finally, the velocity profiles collected in this study could be used to compare the wing efficiency, separation trend, stall effects, circulation strength, vortex location and flowfield characteristics with other MAVs.

Future Recommendations

Although this research was successful in determining the basic characteristics of wing tip displacement and wing tip vortex system, there are some areas for improvement and further research. Some of the test setup and equipment could be altered to improve the reliability of the data. Further analysis of wing displacement and vortex system

should be investigated in the wind tunnel as well as with adequate propulsion system.

Recommendations for the future of this research are:

- To investigate the accurate wing displacement, the survey tool with precision should be utilized and the instrument that can visualize the investigated target should be needed to improve the reliability of the data.

- Mount tri-wire anemometer on a shorter probe which will allow testing in some of the areas that were unable to be measured during this research due to tail and sting interference. This will provide a much more reliable velocity profile and reduce the uncertainty in the momentum balance process.

- Mount propulsion system for MAV. In this study, pure wing aerodynamic characteristics of two MAV models were investigated. However, once the propulsion system is mounted to the MAV models, overall aerodynamic characteristics of the MAV models could be changed. This will allow the MAVs to be tested in more practical situation.

- Collect more velocity data with finer grids and sideslip angles to form the accurate velocity profiles in more flight configurations.

- The MAV will be committed to operations in future. Therefore, the MAV should be tested with various configurations such as camera, transmitter and antenna in wind tunnel as well as in air. These tests will provide practical aerodynamic data for MAV's operations in future.

Appendix : Additional Data Results

Additional Velocity Contour Plots

While the most pertinent results of the wind tunnel velocity profiles are presented in Chapter IV, a few more contour plots were generated during the test runs. Figures 47, 47, 48, 49, 50 and 51 show the additional velocity profile achieved on the right wing for the rigid wing and the flexible wing with tunnel speed set at 30 *mph*.

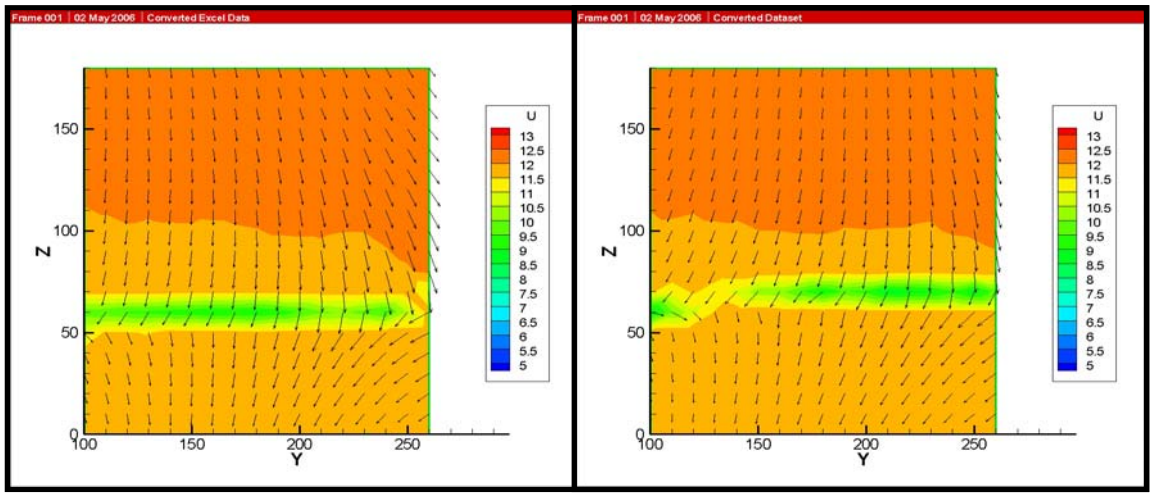

Figure 47. Velocity Profile of Right Wing for Rigid & Flexible Wing at 2° AOA

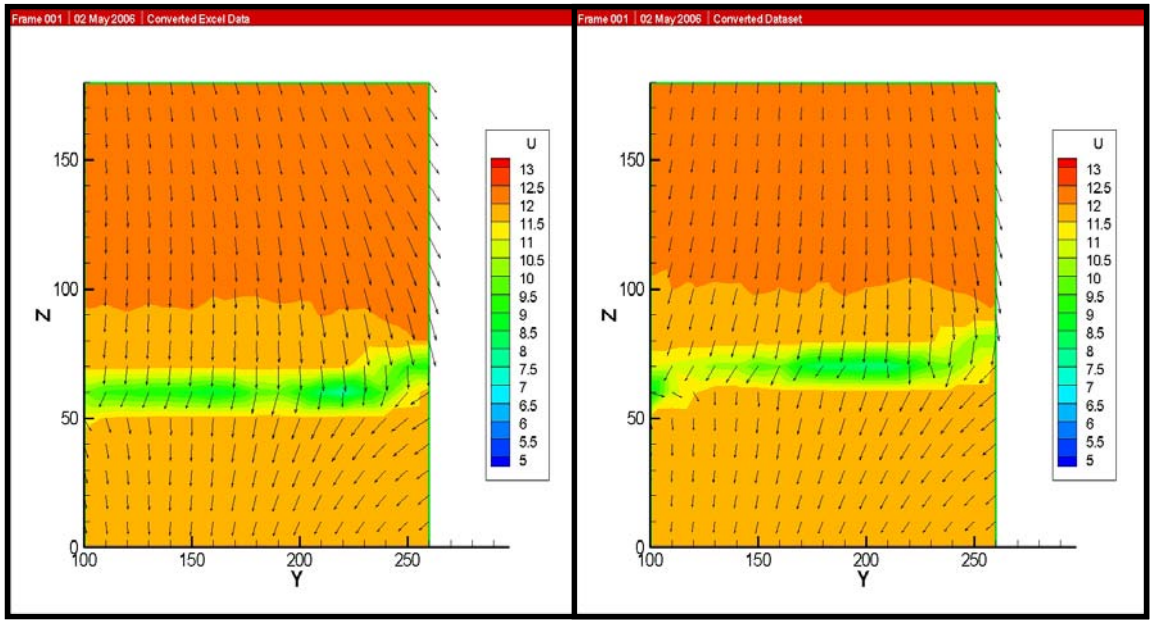

Figure 48. Velocity Profile of Right Wing for Rigid & Flexible Wing at 4° AOA

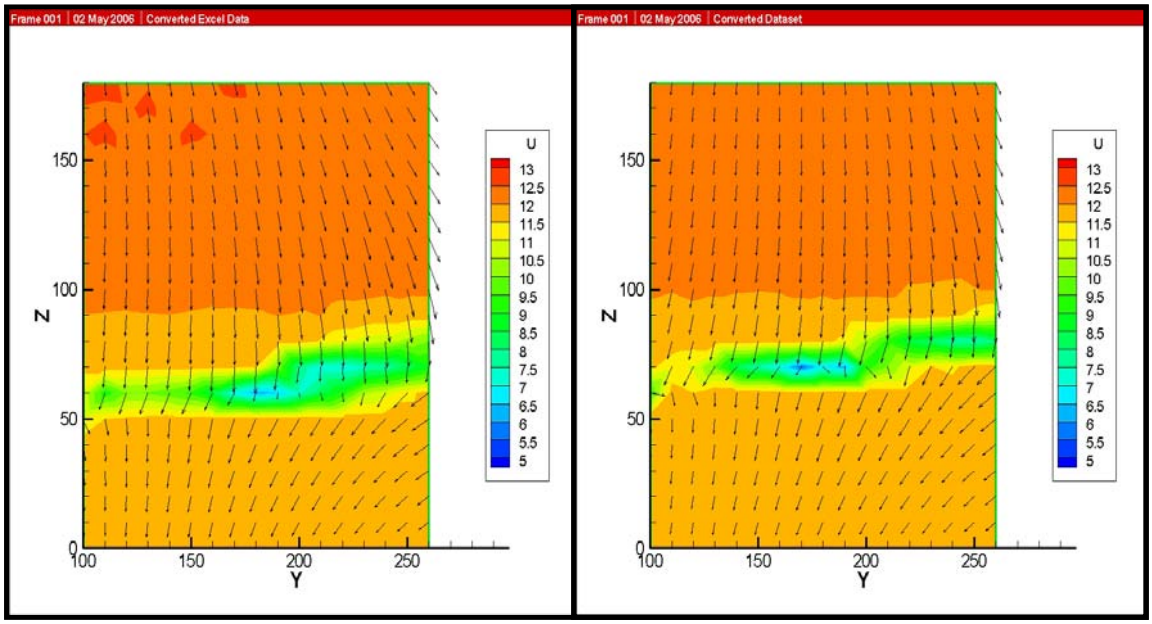

Figure 49. Velocity Profile of Right Wing for Rigid & Flexible Wing at 6° AOA

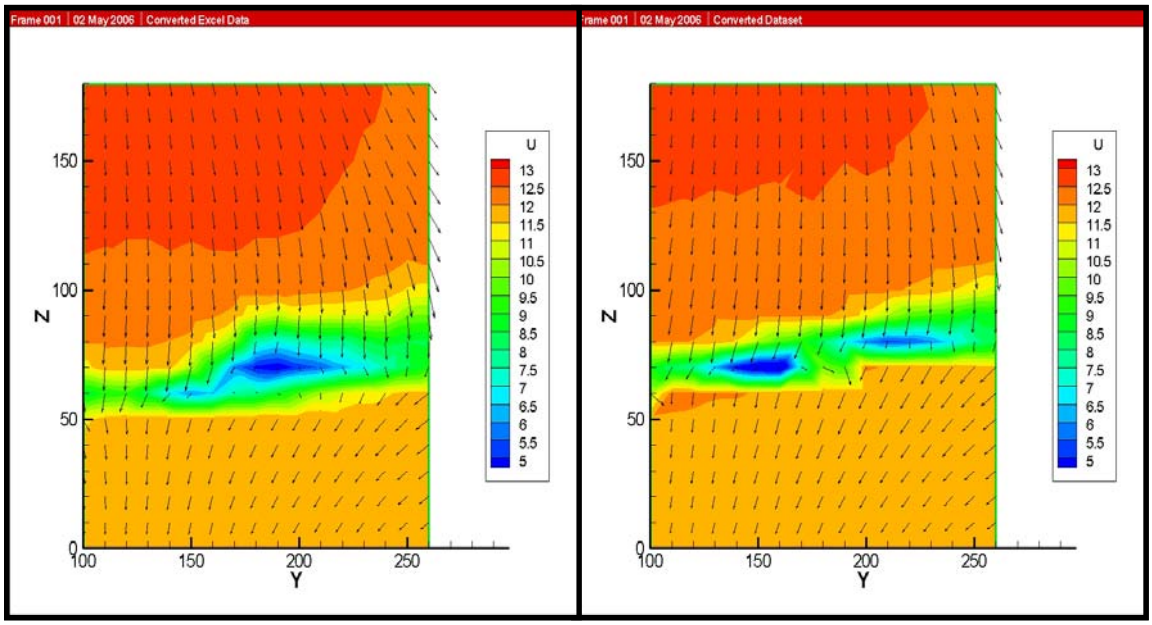

Figure 50. Velocity Profile of Right Wing for Rigid & Flexible Wing at 8° AOA

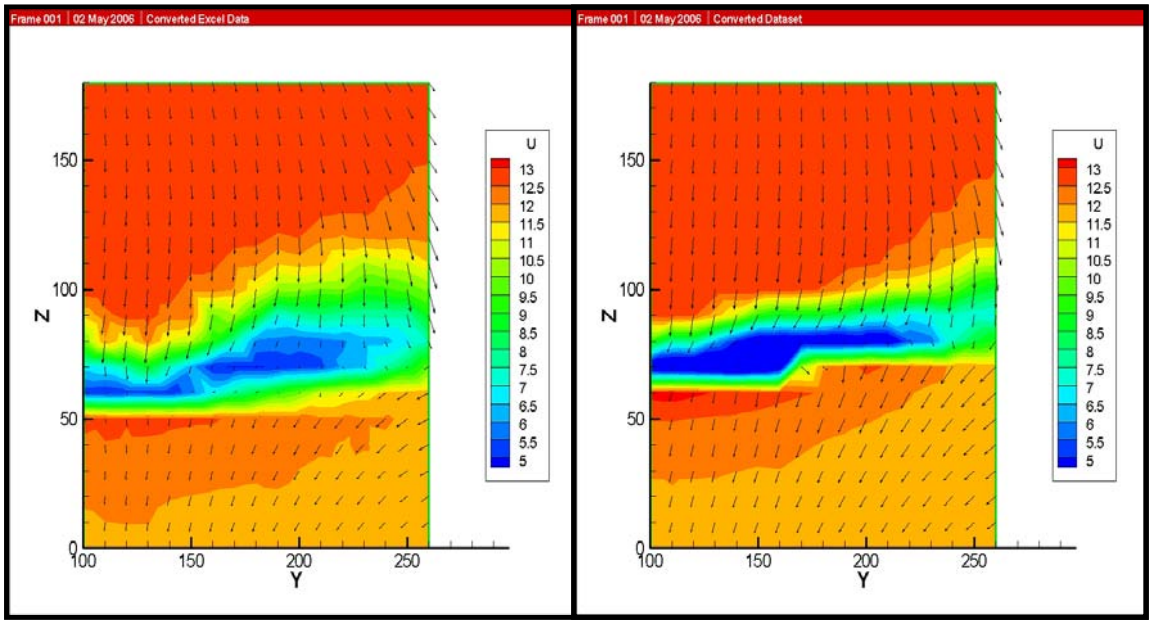

Figure 51. Velocity Profile of Right Wing for Rigid & Flexible Wing at 10° AOA

Additional Variation Velocity Contour Plots with finer grid

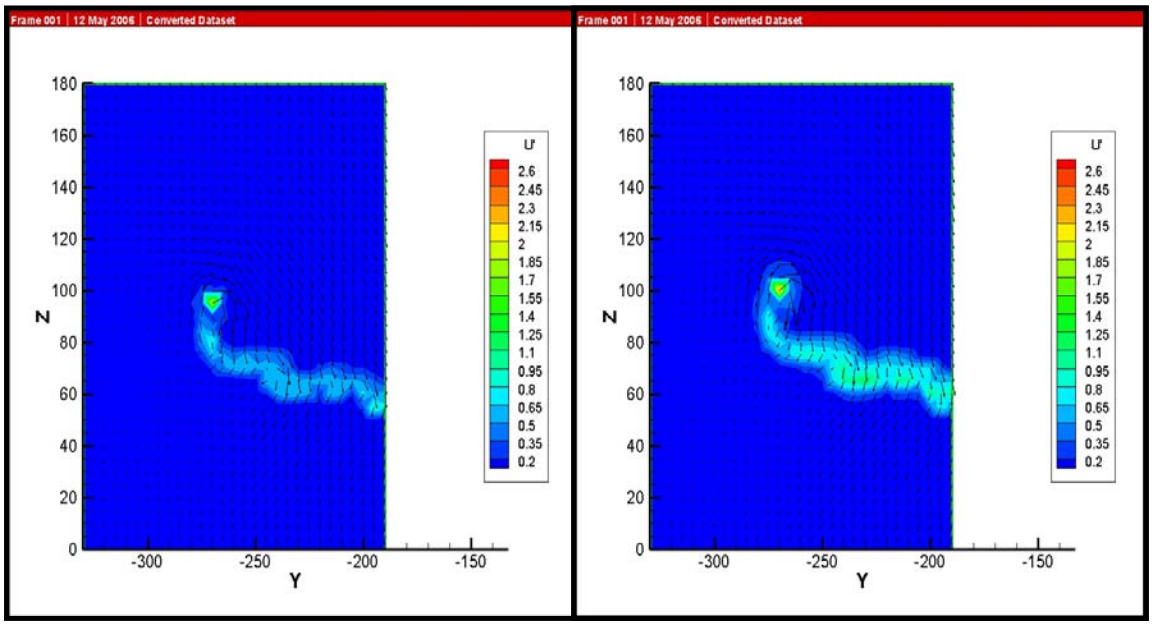

Figure 52. Variation Velocity Profile of Wing Tip for the Flexible Wing at 0°&2° AOA

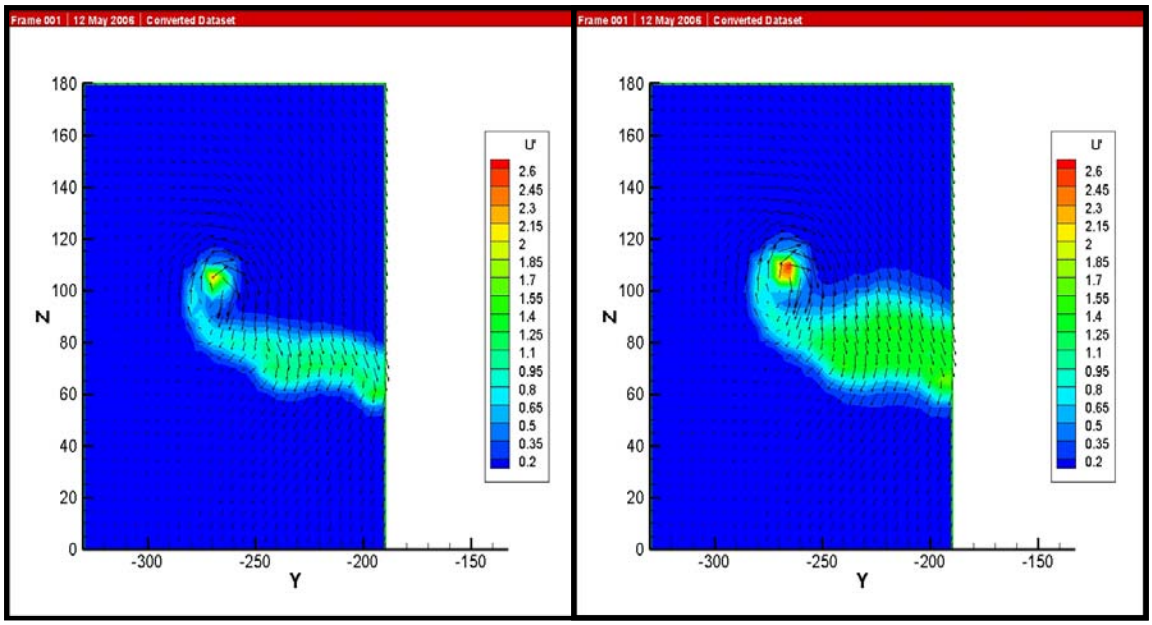

Figure 53. Variation Velocity Profile of Wing Tip for the Flexible Wing at 4°&6° AOA

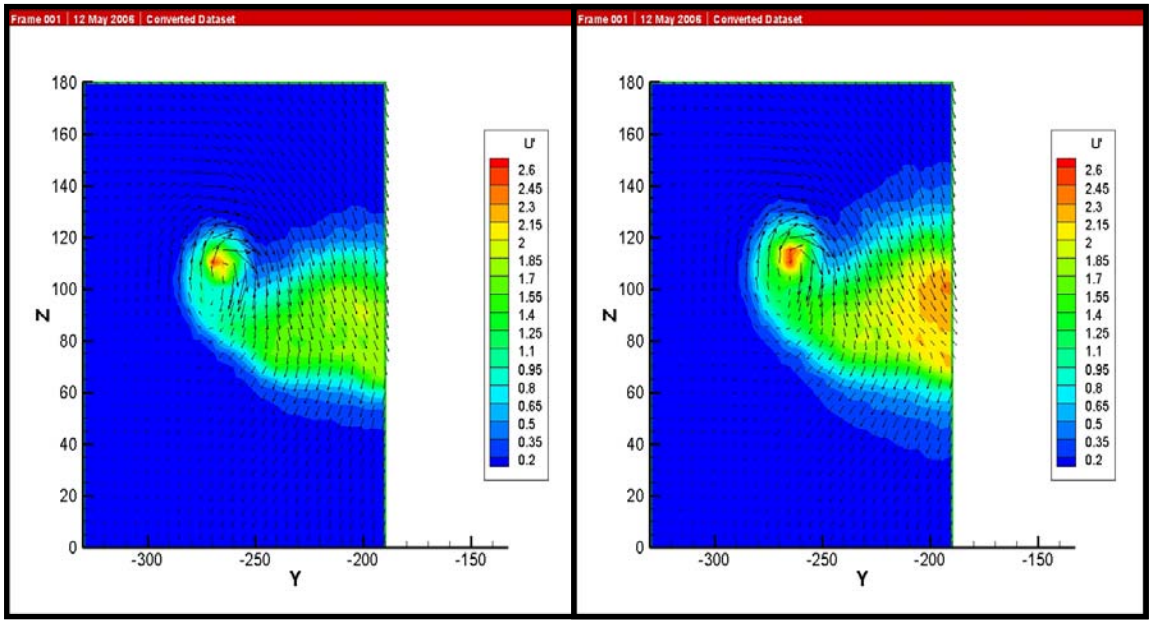

Figure 54. Variation Velocity Profile of Wing Tip for the Flexible Wing at 8°&10° AOA

Bibliography

1. Aerospace web. On line at http://aerospaceweb.org/question/conspiracy/q0274.shtml. accessed 17 May 2006

2. Anderson Elgin A. and Lawton Todd A., "Correlation Between Vortex Strength and Axial Velocity in a Trailing Vortex." *Journal of Aircraft*, Vol. 40, No. 4, 2003: 699-704.

3. Bertin John J. Aerodynamics for Engineers (4th Edition). New Jersey: Prentice Hall Company, 2002

4. Biber K., Ol Michael V. and Tilmann Carl P., "Some Examples of Airfoil Design for Future Unmanned Air Vehicle Concepts." AIAA Paper 2004-1050, (Jan 2004).

5. Bradley S. G., Mursch–Radlgruber E. and S. von Hünerbein, "SODAR Measurements of Wing Vortex Strength and Position." Submitted to J.Ocean. Atmos. Tech. (Oct 2005).

6. Chow Jim S., Zilliac Gregory G. and Bradshaw P., "Mean and Turbulence Measurements in the Near Field of a Wingtip Vortex." *AIAA Journal*, Vol. 35, No. 10, 1997: 1561-1567

7. Dacles-Mariani J., Zilliac Gregory G., Chow Jim S. and Bradshaw P., "Numerical/Experimental Study of a Wingtip Vortex in the Near Field." AIAA Journal, Vol. 33, No. 9, 1995: 1561-1568

8. Dantec Dynamics. Online at http://dantecdynamics.com. Accessed 05 May 2006.

9. Defense Advanced Research Projects Agency. Online at http://www.darpa.mil. Accessed 10 May 2006.

10. DeLuca, Anthony M., "Experimental Investigation into the Aerodynamic Performance of Both Rigid and Flexible Wing Structured Micro Air Vehicles." AFIT Thesis AFIT/GAE/ENY/04-M06, (Mar 04).

11. DeLuca, Anthony M., Reeder, Mark F., OL, Michael V., and Freeman, Jacob, "Experimental Investigation into the Aerodynamic Properties of a Flexible and Rigid Wing Micro Air Vehicle." AIAA Paper 2004.

12. Desktop Aeronautics. On line at http://desktopaero.com/appliedaero/airfoils2/lowresections.html. Accessed 12 May 2006.

13. Deveport William J., Rife Michael C., Liapis Sterios I. and Follin Gordon J., "The Structure and Development of a Wingtip Vortex." *Fluid Mech.*, Vol 312, 1996: 67-106

14. Dryden Flight Research Center. Online at http://www.nasa.gov/centers/dryden/history/pastprojects/Helios/index.html. Accessed 12 May 2006.

15. Federation of American Scientists (FAS). Online at http://www.fas.org/irp/program/collect/mav.htm. Accessed 10 May 2006.

16. Gad-dl-Hak Mohamed, "Micro-Air-Vehicle: Can They be Controlled Better?" *Journal of Aircraft*, Vol. 38, No. 3, 2001: 419- 429.

17. Gamble Brian J., "Experimental Analysis of Propeller Interactions with a Flexible Wing Micro-Air-Vehicle." AFIT Thesis AFIT/GAE/ENY/06-M10, (Mar 06).

18. Ifju, P.G., Jenkins, D.A., Ettinger, S., Lian, Y.,Shyy, W., and Waszak, M.R., "Flexible-Wing-Based Micro Air Vehicles." AIAA Paper 2002-0705, (Jan 2002).

19. Keennon Matthew T. and Grasmeyer Joel M., "Development of the Black Widow and Microbat MAVs and a Vision of the Future of MAV Design." AIAA Paper 2003-2901, (Jul 2003).

20. Leveron, Troy A., "Characterization of a Rotary Flat Tail as a Spoiler and Parametric Analysis of Improving Directional Stability in a Portable UAV." AFIT Thesis AFIT/GAE/ENY/05-J06, (Jun 05).

21. Massachusetts institute of tech. Online at http://www.mit.edu/people/jhow/durip/two%20planes_9.27.03_1.jpg. Accessed 06 Jun 2006.

22. Mathieu J. and Scott J., An Introduction to Turbulent Flow. New York: Cambridge University Press, 2000

23. Raymer, Daniel P., Aircraft Design: A Conceptual Approach (2nd Edition). Washington D.C.: AIAA Education Series, 1992.

24. Rivera Parga, Jose R., Reeder Mark F. and Leveron T., "An Experimental Study of a Micro Air Vehicle with a Rotatable Tail." AIAA Paper 2005-4756.

25. Shyy, W., Klevebring, F., Nilsson, M., Sloan, J., Carroll, B., and Fuentes, C., "Rigid and Flexible Low Reynolds Number Airfoils." *Journal of Aircraft*, Vol. 36, No. 3, 1999: 523-529.

26. Spalart Philippe R., "Airpline Trailing Vortices." *Ann. Review of Fluid Mech*., Vol. 30, 1998: 107-138.

27. University of Adelaide. Online at http://prandtl.maths.adelaide.edu.au/fluids/images/tlv1.jpg. Accessed 10 May 2006.

Vita

REPORT DOCUMENTATION PAGE

Form Approved
OMB No. 074-0188

1. REPORT DATE *(DD-MM-YYYY)*	**2. REPORT TYPE**	**3. DATES COVERED** *(From – To)*
12-06-2006	Master's Thesis	Sep. 2004 – Sep. 2006

4. TITLE AND SUBTITLE

Three Component Velocity Measurements in the Tip Vortex of a Micro-Air-Vehicle

5a. CONTRACT NUMBER

5b. GRANT NUMBER

5c. PROGRAM ELEMENT NUMBER

6. AUTHOR(S)

Hong Joon, Park, Major, ROKAF

5d. PROJECT NUMBER
06-304

5e. TASK NUMBER

5f. WORK UNIT NUMBER

7. PERFORMING ORGANIZATION NAMES(S) AND ADDRESS(S)
Air Force Institute of Technology
Graduate School of Engineering and Management (AFIT/EN)
2950 Hobson Way
WPAFB OH 45433-8865

8. PERFORMING ORGANIZATION REPORT NUMBER
AFIT/GAE/ENY/06-S08

9. SPONSORING/MONITORING AGENCY NAME(S) AND ADDRESS(ES)
Dr. Michael, OL/ AFRL/ VA

2130 8th ST. Bldg. 45, WPAFB, 45433-7542

10. SPONSOR/MONITOR'S ACRONYM(S)

11. SPONSOR/MONITOR'S REPORT NUMBER(S)

12. DISTRIBUTION/AVAILABILITY STATEMENT

APPROVED FOR PUBLIC RELEASE; DISTRIBUTION UNLIMITED.

13. SUPPLEMENTARY NOTES

14. ABSTRACT

The purpose of this research was to improve the MAV that will be used for battle damage assessment and reconnaissance or local surveillance through the experiments in AFIT wind tunnel. The experiments were performed to investigate the wing displacement and wing tip vortex interaction. To conduct the experiments, telescopic survey tool and tri-axial hot-wire anemometer was utilized. The results indicate that wing tip displacement of the flexible wing was approximately 8 times that of the rigid wing in an unstalled condition and data suggests that flexible wing has a denser core-distribution of velocity within the wing tip vortex and delays the angle at which separation occurs.

15. SUBJECT TERMS
Wing Tip Displacement, Tip Vortex, Axial Velocity, Circulation, Hot-wire anemometer

16. SECURITY CLASSIFICATION OF:			**17. LIMITATION OF ABSTRACT**	**18. NUMBER OF PAGES**	**19a. NAME OF RESPONSIBLE PERSON**
a. REPORT	**b. ABSTRACT**	**c. THIS PAGE**			Dr. Mark F. Reeder
U	**U**	**U**	**UU**	88	**19b. TELEPHONE NUMBER** *(Include area code)* (937) 255-6565, ext 4350; Mark.Reeder@afit.edu

Standard Form 298 (Rev. 8-98)
Prescribed by ANSI Std. Z39-18